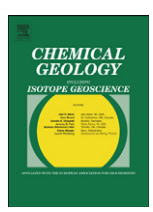
FISEVIER

Contents lists available at ScienceDirect

Chemical Geology

journal homepage: www.elsevier.com/locate/chemgeo



Trapped-charge thermochronometry and thermometry: A status review



Georgina E. King ^{a,*}, Benny Guralnik ^b, Pierre G. Valla ^c, Frédéric Herman ^c

- ^a Institute of Geography, University of Cologne, 50923, Germany
- b Soil Geography and Landscape group and the Netherlands Centre for Luminescence Dating, Wageningen University, Droevendaalsesteeg 3, 6708PB Wageningen, The Netherlands
- ^c Institute of Earth Surface Dynamics, University of Lausanne, CH-1015, Switzerland

ARTICLE INFO

Article history: Received 28 September 2015 Received in revised form 16 August 2016 Accepted 18 August 2016 Available online 20 August 2016

Keywords:
Low-temperature thermochronometry
Thermometry
Trapped-charge dating
Electron spin resonance (ESR)
Thermoluminescence (TL)
Optically stimulated luminescence (OSL)
Infra-red stimulated luminescence (IRSL)

ABSTRACT

Trapped-charge dating methods including luminescence and electron spin resonance dating have high potential as low temperature ($<100\,^{\circ}$ C) thermochronometers. Despite an early proof of concept almost 60 years ago, it is only in the past two decades that thermoluminescence (TL), electron-spin-resonance (ESR), and optically stimulated luminescence (OSL), have begun to gain momentum in geological thermochronometry and thermometry applications. Here we review the physics of trapped-charge dating, the studies that led to its development and its first applications for deriving palaeo-temperatures and/or continuous cooling histories. Analytical protocols, which enable the derivation of sample specific kinetic parameters over laboratory timescales, are also described. The key limitation of trapped-charge thermochronometry is signal saturation, which sets an upper limit of its application to $<1\,$ Ma, thus restricting it to rapidly exhuming terrains ($>200\,^{\circ}$ C Ma $^{-1}$), or elevated-temperature underground settings ($>30\,^{\circ}$ C). Despite this limitation, trapped-charge thermochronometry comprises a diverse suite of versatile methods, and we explore potential future applications and research directions.

© 2016 Elsevier B.V. All rights reserved.

1. Introduction

The need to constrain the rate and timing of landscape evolution has led to a continuous growth of thermochronometric techniques, which quantify the thermal histories of rocks (Reiners and Ehlers, 2005). A suite of methods are applicable to different temporal and spatial scales. however constraining recent (<1 Ma) thermal histories at temperatures <100 °C remains challenging. Luminescence and electron-spin-resonance (ESR) dating are trapped-charge dating methods whose thermal sensitivities can span this temporal gap. They are based on the quantification of free electric charge (electrons and holes), which become trapped in the proximity of various defects and impurities in the crystalline lattice of minerals (e.g. quartz, feldspar) as a result of their exposure to environmental radiation (cf. Aitken, 1985). This charge can be evicted by exposure of the crystal to external energy such as heat, light and/or pressure, and hence its concentration can be related to the last exposure of natural materials to high temperature (Aitken et al., 1968; Brown et al., 2009). Therefore, trapped-charge techniques can be used to gain insights into the thermal histories of rocks.

Although the possibility of interpreting trapped charge within natural crystals as records of their thermal histories was initially demonstrated more than half a century ago (Houtermans et al., 1957), this technique received only marginal attention from the geological community, initially for surface palaeothermometry (e.g. Ronca and Zeller,

* Corresponding author.

E-mail address: georgina.king@gmail.com (G.E. King).

1965), and later for characterising lunar surface temperatures (e.g. Durrani et al., 1977). With an increasing interest for quantifying recent stages of rock thermal histories from the thermochronological community (Reiners and Ehlers, 2005) and the need to constrain the rate and timing of landscape evolution during the Quaternary, trapped-charge dating methods utilising ESR, thermoluminescence (TL), and optically stimulated luminescence (OSL) were (re)investigated in the context of low-temperature thermochronometry (Grün et al., 1999; Tsuchiya and Fujino, 2000; Herman et al., 2010; Guralnik et al., 2015a; King et al., 2016a). In particular, OSL-thermochronometry has been the focus of rapid development since its introduction in 2010, and has come to be recognized as a new developing field of luminescence dating (Duller, 2015a, 2015b; Roberts and Lian, 2015). In its simplest form, trappedcharge thermochronometry comprises constraining the interplay between (i) the rate of charge trapping, due to exposure to ionising radiation, and (ii) the rate of charge detrapping, due to temperature (Christodoulides et al., 1971). By constraining charge trapping and detrapping rates on a sample-specific basis, the natural concentrations of trapped charge can be translated into ages and their corresponding palaeotemperatures.

Here we aim to provide a brief overview of the underlying physics of trapped-charge dating, describe the common equipment and key measurements of each sub-technique, and trace the development of trapped-charge thermochronometry from early pioneering studies to the current state-of-the-art. At a time when a range of new low-temperature thermochronometric techniques are under development (e.g. Tremblay et al., 2014; Shuster and Cassata, 2015; Amidon et al., 2015),

it is particularly interesting to review trapped-charge dating methods with comparable thermal stabilities, that could be used in conjunction with the above geochemical methods to obtain even higher-resolution palaeotemperature constraints, inaccessible when using each method independently.

2. Physical principles

2.1. Electron traps in a crystalline lattice

Both luminescence and ESR dating are based on the measurement of trapped electrons, which build up in crystal defects (Fig. 1A) due to naturally-occurring ionising radiation. Such defects or imperfections include atomic interstitials, atomic vacancies and elemental substitutions. Even the purest crystals contain defects, and even impurity concentrations of the order of 10^{-3} ppm can result in defect concentrations of $\sim 10^{13}$ cm⁻³ (Preusser et al., 2009). When ionising radiation from alpha, beta or gamma decay, as well as from cosmic radiation, interacts with the crystalline lattice (Fig. 1B), sufficient energy may be transferred to some bonding electrons, causing them to detach from their sites; once mobile, free electrons diffuse towards positivelycharged defects and impurities within the crystal. Conversely, each evicted electron leaves a 'hole' behind (a lack of an electron; a virtual particle with a charge of e⁺) which experiences an analogous diffusion towards negatively-charged defects and impurities. Once in their traps, electrons and holes remain immobile until thermal lattice vibrations give electrons sufficient energy to escape, allowing them to diffuse again through the crystal (Fig. 1C) and to recombine with trapped holes. Upon electron-hole recombination, excess energy is released either in the form of measurable light (luminescence) or dissipated as heat in the crystal. For more in-depth descriptions of electron and hole trapping and detrapping in quartz and feldspar minerals, the reader is referred to e.g. Aitken (1985); Chen and Pagonis (2011), and Jain and Ankjærgaard (2011).

Although the precise defects that give rise to OSL and TL from quartz are still the subject of investigation (e.g. Yang and McKeever, 1990; McKeever, 1991; Martini et al., 2009; Preusser et al., 2009), the UV-blue emissions which are typically measured from quartz have been associated with the substitution of Si⁴⁺ with Al³⁺, this charge deficit being compensated by Li⁺, Na⁺ (Perny et al., 1992), H⁺ (Itoh et al., 2002; Luff and Townsend, 1990) or a trapped hole (h⁺) (Martini et al., 1995, 2009). Quartz also contains many paramagnetic centres that can be exploited in ESR dating, although usually only the Al and Ti centres are targeted (cf. Skinner, 2011; Blackwell et al., 2016). Finally, the source of the blue emission of feldspar in response to infra-red stimulation (termed IRSL, but broadly falling within the OSL category) remains understudied but has been associated with Al-O-Al centres (Finch

and Klein, 1999). The reader is referred to Krbetschek et al. (1997) for a detailed review of luminescence emissions from quartz and feldspar minerals.

An electron-hole pair may be produced by any naturally occurring alpha, beta, gamma or cosmic radiation. The sample's natural radioactivity from all accountable sources is usually expressed as the natural dose rate (\dot{D}), with unit of Gray per unit time (e.g. Gy s⁻¹ or Gy ka⁻¹). Conversely, the product *n* is the number of trapped electrons at any given time (see Table 1 for a short nomenclature guide). Since the number of crystal defects/impurities is finite, the amount of electrons that can become trapped is also limited. Consequently, out of *N* electron traps of a certain kind with $n \le N$ electrons in them, only the empty sites (N-n) can attract newly produced charge (Klasens and Wise, 1946). This 'space limitation' is a key phenomenon in trapped-charge geoand thermochronometry (cf. Li and Li, 2012; Guralnik et al., 2013) which generally results in signal saturation over timescales exceeding 10⁵ years (Wintle, 2008). While some ESR centres or OSL traps may exhibit significantly later saturation (i.e. up to 10⁶ years; Rink, 1997; Ankjærgaard et al., 2015), all trapped-charge systems seem to eventually be affected by the saturation phenomenon (Grün, 2001).

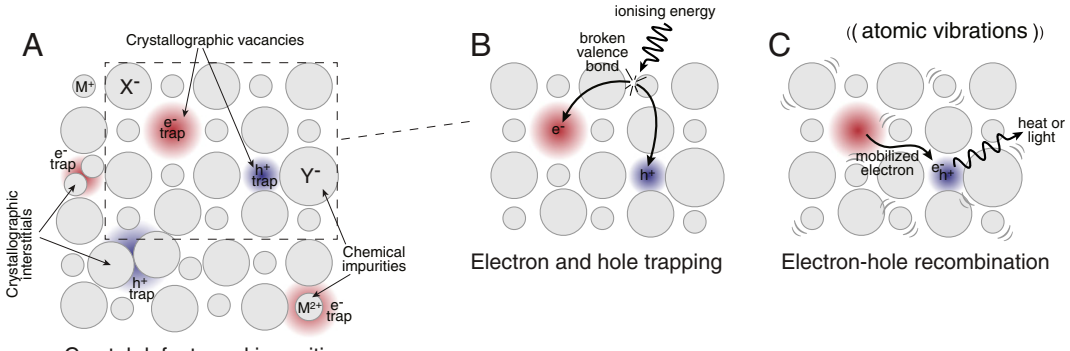
Various minerals, mineral defects and impurities have different trapping capacities and thermal stabilities (see Table 2 for some representative values). Therefore, trapped-charge thermochronometry comprises a versatile suite of different stability systems, with thermal sensitivity in the ~40–100 °C range (e.g. Grün et al., 1999; Wu et al., 2015; Guralnik et al., 2015a; Ankjærgaard et al., 2015; King et al., 2016a). Furthermore, these systems can be used in combination to provide multi-thermochronometric constraints (Qin et al., 2015; King et al., 2016a), enabling the derivation of continuous cooling histories. Trapped-charge techniques therefore lend themselves to a diverse range of applications including thermometry (Christodoulides et al., 1971), thermochronometry (Toyoda and Ikeya, 1991), and constraint of instantaneous cooling or reheating events (see reviews by Fleming, 1979; Bailiff, 2015; Tsukamoto, 2015).

2.2. Mathematical description

The most basic mathematical description of the simultaneous electron trapping and detrapping, which occurs in a crystal exposed to environmental radiation and heat, is given by:

$$\frac{dn}{dt} = p_{trapping} (N-n) - p_{detrapping} n \tag{1}$$

in which t (s) is time, (N-n) and n the unitless number of empty and occupied electron traps respectively, and $p_{trapping}$ and $p_{detrapping}$ the probabilities of an electron occupying and vacating a trap per unit



Crystal defects and impurities

Fig. 1. Schematic diagram of charge trapping and release. (A) A crystalline alkali-halide lattice, depicting common lattice imperfections such as vacancies, interstitials, and impurities. (B) Trapping and (C) detrapping of an electron-hole pair (e⁻ and h⁺ respectively) in the crystal due to the effects of radiation and temperature, respectively. In (B) ionization of an electron results in diffusion of e⁻ to an electron trapping site, and of h⁺ to a luminescence recombination centre. Exposure of the mineral to heat (C) enables the electron to escape the trapping site and to recombine with a hole, leading to a release of excess energy either in the form of measurable light (luminescence signal), or via dissipation by heat.

Table 1Trapped-charge dating nomenclature guide.

Parameter	Units	Definition					
\dot{D} , dose rate $\begin{array}{c} \text{Gy s}^{-1} \text{ or } \\ \text{ka}^{-1} \end{array}$		The effective amount of energy (Gy = J kg ⁻¹) per unit time, deposited within a crystal due to naturally occurring radioactivity. A distinction can be made between internal and external dose rates: the former arises from radionuclides within the target crystal, the latter from its surrounding matrix and environment. Characteristic internal dose rates of selected minerals of interest are cited below (after Templer, 1986; Vandenberghe et al., 2008; Sohbati et al., 2013): ~0.2 mm Quartz with 80 ppb U and 180 ppb Th: ~0.01 Gy ka ⁻¹ . ~0.5 mm Na-feldspar with 3% internal K content: ~0.5 Gy ka ⁻¹ . ~0.5 mm K-feldspar with 12.5% internal K content: ~2 Gy ka ⁻¹ . 0.1–0.4 mm zircon with 100 ppm U and 100 ppm Th: ~50 Gy ka ⁻¹ . External dose rates arise both from the chemistry of the surrounding environment, as well as the cosmic radiation. Crystalline rocks of mafic (e.g. amphibolite) and felsic (e.g. gneiss) lithology generally have external dose rates of ~1 and ~3 Gy ka ⁻¹ , respectively, although more extreme values in the range 0.5–10 Gy ka ⁻¹ can sometimes be encountered. At the surface, the cosmic radiation is of the order of ~0.2 Gy ka ⁻¹ , usually amounting to a negligible contribution in bedrock lithology.					
D_e , equivalent dose	Gy	The equivalent radiation dose that the sample has received in nature. Obtained via interpolation of the natural TL/ESR/OSL signal onto a laboratory dose-response curve (regenerative protocols; Fig. 2G–I), or via extrapolation of the dose response to zero dose (in additive protocols). D_r is functionally related to n/N (see below) but is easier to obtain.					
<i>n/N</i> , fraction of saturation	unitless	The fraction of occupied electron traps (unitless), varying between 0 (all empty) and 1 (all full, or saturated). Mathematically, n/N is equivalent to the ratio D/P between a radiogenic daughter nuclide (D) and its radioactive parent isotope (P) (cf. Braun et al., 2006). Due to uncertainties in the precise level of signal saturation, signals within 15% of saturation cannot be reliably distinguished from "infinitely old", and are thus reported as minimum ages.					
D ₀ , characteristic dose	Gy	The cumulative dose, at which the target dosimetric trap fills to \sim 63% (1-e ⁻¹) of its full capacity. The reciprocal, D_0^{-1} , can be thought of as the probability of populating an electron trap per unit dose. Typical values are in the 100–1000 Gy range, although more extreme values can be sometimes seen (e.g. in ESR, where signal saturation is seen only at extreme doses in the kGy range).					
\dot{D}/D_0 , trapping rate	s ⁻¹ or ka ⁻¹	The electron trapping rate per unit time. Mathematically, \dot{D}/D_0 is equivalent to the decay lifetime ($\lambda = \ln(2)/t_{1/2}$) of a short-lived parent. As such, the time required to fill half of the remaining empty traps can be calculated from $t_{1/2} = \ln(2)D_0/\dot{D}$. Characteristic values based on Table 2 are $t_{1/2} \sim 100$ ka for TL, $\sim 1-2$ Ma for ESR, and 40–60 ka for OSL.					
E, trap depth	eV	The energy required to excite the electron from its trap to the electrical conduction band (where it is infinitely mobile), or to a band tail (where its mobility is finite). Trap depths [eV] may be translated into equivalent activation energies [k]/mol] via multiplication by 96.49 (Avogadro's number times 1 eV = 1.6×10^{22} kJ). Thus, as a rule of thumb, characteristic electron trap depths of ~1–2 eV correspond to activation energies of ~100–200 kJ/mol.					
s, frequency factor	s^{-1}	The number of times that a trapped electron attempts to escape its trap, per unit time. Identical to the escape frequency Ω in noble gas thermochronometry.					
g-value (anomalous fading)	%/decade	A laboratory measure of the athermal loss of electrons due to quantum mechanical tunnelling. This is a competing pathway to thermal loss that can lead to severe "cooling rate artefacts" if not accounted for properly. g-values reflect fractional signal loss (hence $%$) as a function of $\log_{10}(\text{time})$ (hence "decade"), and are typically normalised to cumulative loss over 2 days (Huntley and Lamothe, 2001).					
T_c , closure temperature	°C	Given a cooling path, and a determined age A , T_c is the corresponding palaeotemperature, which the sample experienced A years ago. Due to saturation effects, T_c evaluation in trapped charge systems differs from that in standard thermochronometry (cf. Guralnik et al., 2013). In the general case of nonlinear kinetics, closure temperatures should be evaluated numerically, by projecting a calculated age back in time onto the time-temperature history, to read off the corresponding palaeotemperature.					

time respectively. Since the absolute value of N (the actual number of available traps) is difficult to measure, it is convenient to describe the system in terms of n/N (the 'fraction of saturation'), varying between 0 (all traps vacant) and 1 (all traps occupied). Note that n/N is mathematically equivalent to the daughter/parent ratio in fission-track and noble gas thermochronometry (Table 1).

In the simplest first-order kinetic model (Christodoulides et al., 1971), the electron trapping probability $p_{trapping}$ is constant, while the detrapping probability $p_{detrapping}$ depends on temperature following an Arrhenius-type expression:

$$p_{trapping} = \dot{D}/D_0, p_{detrapping}(T) = s e^{-E/k_BT} \tag{2}$$

in which \dot{D} (Gy s⁻¹) is the dose rate, D_0 (Gy) is the characteristic (or 'saturation') dose, T (K) is temperature, E (eV) and s (s⁻¹) are the activation energy and escape frequency of the trap (respectively), and k_B is Boltzmann's constant. Eqs. (1)–(2) serve as a baseline for addressing the primary dynamics of all trapped-charge systems (Guralnik et al., 2013 and references therein). However, often a more complex, nonfirst-order or multi-exponential model is required to sufficiently describe the processes of electron trapping and detrapping in a given mineral (cf. Guralnik et al., 2015c).

Apart from signal saturation, a second fundamental characteristic of trapped-charge thermochronometry is the fact that $p_{detrapping}$ may be governed not only by an Arrhenius-like thermal activation, but by an additional athermal (or weakly-thermal) loss, commonly referred to as 'anomalous fading' (Wintle, 1973). Anomalous fading occurs when a trapped electron recombines with its nearest-neighbouring hole, without having overcome the energy barrier to escape its trap. This is

thought to occur via quantum mechanical tunnelling (Delbecq et al., 1974; Visocekas et al., 1976), which theoretically has no thermal dependence, but which may sometimes be indirectly linked to weak thermal effects (e.g. Jain et al., 2013). Anomalous fading is ubiquitous in feldspar (Huntley and Lamothe, 2001; Huntley and Lian, 2006; Valla et al., 2016) but rare in quartz, and is thought to relate both to the chemical composition (e.g. Akber and Prescott, 1985) as well as the degree of lattice structural order (Wintle, 1973; Spooner, 1994; Tsukamoto et al., 2007) of a given mineral. To account for trapped-charge build-up under combined thermal and athermal loss, Eq. (2) can be in the simplest case extended to:

$$p_{trapping} = \dot{D}/D_0, p_{detrapping}(T) = s e^{-E/k_B T - \alpha r}, \tag{3}$$

(cf. Mott, 1969; Jain et al., 2013; Guralnik et al., 2015a), in which α (m $^{-1}$) is a constant (related to Bohr's radius), and r (m) the distance from a trapped electron to its nearest neighbouring hole (Huntley, 2006). While systems involving both thermal and athermal losses, e.g. as described by Eqs. (1) and (3), often require numerical (rather than analytical) solutions, they do inherit all of their fundamental properties and behaviours from simpler, first-order models.

2.3. Methods for quantifying trapped charge

A thermoluminescence measurement (Fig. 2A,D) consists of recording the emission of light from the target material (e.g. crystal or crystals) in a certain spectral window using a photomultiplier tube or a photon counter, while the sample is gradually heated (usually at a linear rate). The maximum temperatures that samples are ramped to are

Table 2Representative kinetic parameters of some trapped-charge thermochronometers.

Method	Mineral	Signal	(Gy ka ⁻¹)	D_0 (Gy)	<i>E</i> (eV)	s (s ⁻¹)	Detectable cooling rate (°C Ma ⁻¹)
TL	Quartz	375 °C peak ^{a §}	1.6	250	1.87	5.0×10^{14}	>265
		425 °C peak ^{a §}	1.6	250	1.83	1.0×10^{13}	>320
ESR	Quartz	Al centre ^{b †}	1.1	3300	1.70	1.1×10^{7}	>25
		Ti centre ^{b †}	1.1	2200	1.70	4.1×10^{11}	>20
OSL	Quartz	Fast component c †	1.3	80	1.59	1.8×10^{13}	>380
	Na-feldspar	IRSL ₅₀ d †‡	2.4	210	1.70	3.2×10^{14}	>300
	K-feldspar	pIRIR ₂₂₅ e †‡	8.4	690	1.58	5.4×10^9	>615

Kinetic parameters due to: a) Gong et al. (2010) and references therein; b) Tsukamoto et al. (2015) and references therein; c) Wu et al. (2015); d) Guralnik et al. (2015a), 2015b, 2015c); e) King et al. (2016a). § Scarce kinetic data. † Non-first-order kinetics. ‡ Anomalous fading. Detectable cooling rates have been calculated using Eqs. (1)–(2) and assuming first-order kinetics; such obtained values are guidelines only.

~500-600 °C, marking the transition to blackbody radiation, which overprints any remaining luminescence signals. In an OSL measurement (Fig. 2C.F), the target material is stimulated with a certain wavelength. and optically detected using a photomultiplier tube or a photon counter in a shorter wavelength, corresponding to a higher energy than the stimulating source (i.e. anti-Stokes emission). While optical stimulation may involve pulsing or modulation of either intensity or wavelength, most current protocols deploy continuous wave stimulation at a fixed wavelength. Both TL and OSL are most commonly measured using automated systems, such as the Risø TL/OSL (Bøtter-Jensen et al., 2000) or Lexsyg (Richter et al., 2013) luminescence readers, which include internal heating, irradiation, light stimulation and light detection facilities with variable setups and with capacity for up to 80 samples. Both TL and OSL measurements are destructive, in the sense that they quantify trapped charge through its eviction from the corresponding traps (converting a proportion of the evicted electrons to light).

An ESR measurement (Fig. 2B,E) consists of measuring the absorption of microwave radiation (using a detector diode) as a function of the magnetic field strength (Skinner, 2015). In contrast to OSL/TL measurements, ESR measurements are non-destructive, meaning that the measurement does not involve eviction of trapped charge, but rather measurement of the resonance of electron energy states stimulated by application of an external magnetic field. The ESR of quartz is usually measured using a Bruker or Jeol X- or Q-band ESR-spectrometer (e.g. Tsukamoto et al., 2015) and importantly measurement of the Al or Ti centres must be done at low temperatures (~80–110 K).

Luminescence and ESR signals can be measured using a range of different protocols. The common feature to all such protocols is that they strive to relate the signal of the natural trap population (curves marked as 'Nat.' in Fig. 2D-F) to laboratory-regenerated signals due to known radiation doses. A further important distinction can be made between regenerative dose protocols, in which traps are first emptied and then artificially refilled to different extents (curves R₁–R₃ in Fig. 2D–F), and additive dose protocols, in which the natural trap population is preserved and further supplemented via irradiation. Since the amount of absorbed (equivalent) dose is estimated from relating natural to artificial (laboratory-induced) signals, the choice between regenerative and additive dose protocols often hangs on their ability to artificially reproduce as many possible features and characteristics of the natural signal, in the signals due to known doses. A failure to do so often invalidates the interpolation of the natural signal onto laboratory behaviour, due to unconstrained sensitisation of the sample during the measurement cycles. The dose response experiments visualised in Fig. 2D-F and quantified in Fig. 2G–I were all obtained using a regenerative dose method.

3. Analytical procedures

3.1. Sample preparation

Samples for trapped-charge thermochronometry generally comprise bedrock material sampled at the surface of the Earth or from within boreholes or tunnels. Because investigated signals are light sensitive, at least 1 cm of material is removed from the sample's surface under subdued red light conditions, to ensure that only light-unexposed material is analysed (Liritzis, 2011; Sohbati, 2015 and references therein). Samples are gently hand crushed to avoid potential signal resetting by grinding (e.g. Bateman et al., 2012), before preparation using standard laboratory procedures. These include sieving to isolate a grain size for measurement (typically ~180–250 μm), chemical treatment with HCl and H₂O₂ to remove carbonates and any organic material, respectively, and density separation to isolate the quartz $(<2.68 \text{ g cm}^{-3})$ and feldspar $(<2.62 \text{ g cm}^{-3})$ mineral fractions from typically heavier minerals. Finally, quartz minerals are etched in concentrated HF to remove feldspar contamination and the majority of the alpha-irradiated outer part of the quartz grains. Feldspar grains may also be etched (e.g. Li and Li, 2011a) although it has been shown that etching of feldspar does not result in removal of an isotropic layer (Duller, 1992). This means that although some of the alpha dose will be removed, an unknown portion of that dose may remain, potentially affecting age (or cooling rate) determinations. When grains are not etched, the contribution of the alpha dose rate can be accounted for using alpha efficiency factors (cf. Kreutzer et al., 2014).

3.2. Constraining the natural trapped-charge population: dose response

In trapped-charge dating, the accumulated dose in nature (called the equivalent dose, D_e) is quantified through measuring the natural luminescence signal and interpolating it onto, or from, a laboratory-generated dose response curve (Fig. 2G-I). Trapped-charge measurements benefit from a series of internal checks which enable control of data quality, many of which are incorporated within standard measurement protocols (e.g. the ability to measure the dose reproducibly or to recover a given dose; e.g. Murray and Wintle, 2000, 2003). In trapped-charge thermochronometry, it is crucial not only to measure the natural accumulated dose, but also to characterise the rate at which the signal saturates, and its saturation level. In some cases, determining signal saturation can be challenging, partly because at high doses, artificial irradiation may introduce laboratory artefacts that are generally not observed in natural and independently dated archives (cf. Chapot et al., 2012; Timar-Gabor and Wintle, 2013; Duval and Guilarte, 2015). Fig. 2G-I show characteristic dose response curves for TL of bulk calcite (Zeller and Ronca, 1963), ESR of quartz (Toyoda and Ikeya, 1991) and OSL of feldspar (Guralnik et al., 2015a). As can be seen in all plots, signal saturation, or a considerable growth deceleration, is reached in all experiments and can be well-constrained; as discussed below (Section 6.1), the level of saturation and the rate at which it is reached define the characteristic lifetime of the dating system, which unlike in noble gas or for fission-track products is finite (Table 1). Quartz OSL often exhibits a first-order dose response (e.g. Wintle and Murray, 2006; Wu et al., 2015), while dose response in feldspar can require multi-exponential fitting (see Guralnik et al., 2015c for a review).

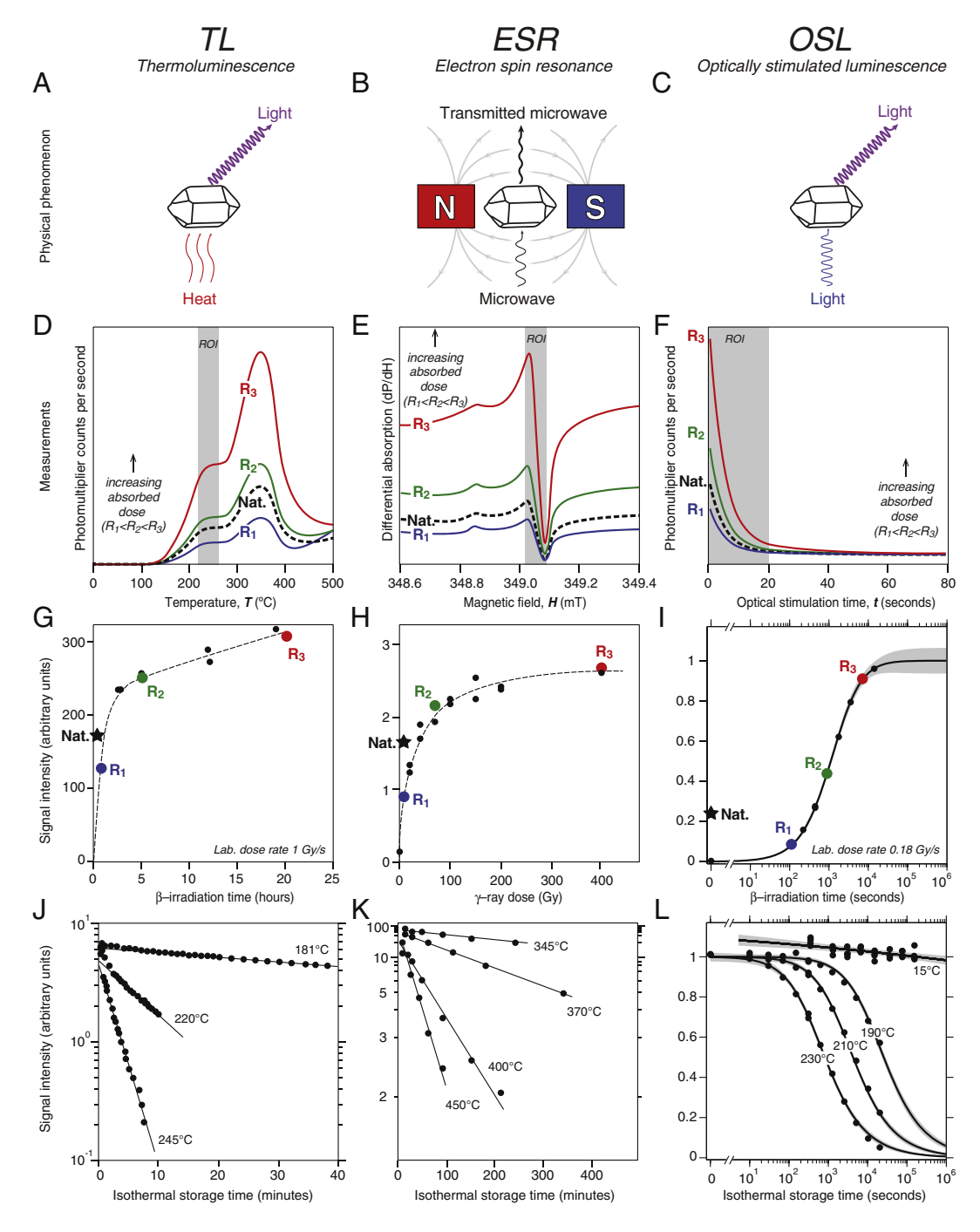


Fig. 2. Physical processes and measurements of different trapped-charge dating systems. (A) Stimulation of TL using heat, (B) ESR using microwaves and (C) OSL using light. (D–F) Signals measured for the different techniques. The natural signals are shown as dashed lines (Nat), whereas coloured lines show the response to different regenerative (R_1 – R_3) laboratory doses; all growth curves were obtained after zeroing the natural signal by thermal/optical stimulation. Note that the ESR spectra are offset from one another for clarity (E). Grey shading highlights the region of interest (ROI) over which the signals are integrated, to construct the laboratory dose response curves shown in (G–I). The dose response curve for TL is redrawn from Zeller and Ronca (1963, G), for ESR from Toyoda and Ikeya (1991, H) and for OSL from Guralnik et al. (2015a, I). The laboratory measured doses that accumulated in nature (stars in G–I) are interpolated onto their respective dose response curves to determine the *fraction of saturation* (n/N) or *the equivalent dose* (D_e). Note that these values were not provided in the original publications of Zeller and Ronca (1963) and Toyoda and Ikeya (1991) but are added here for illustrative purposes. Similarly the coloured circles which relate to the first (R_1), second (R_2) and third (R_3) regenerative doses in (D–F) are illustrative. (J–L) In addition to measuring the equivalent dose, signal loss in response to thermal stimulation must also be constrained. This is done through measuring signal loss in response to different durations of isothermal storage, figures are redrawn from the same studies as for (D–I). Finally, for feldspar minerals, athermal losses related to anomalous fading must also be measured (15 °C isothermal storage, L).

3.3. Constraining thermal and athermal loss: isothermal decay

There are many ways to determine the thermal kinetic parameters of a particular trapped-charge signal (e.g. Prokein and Wagner, 1994), but the method which is most comparable to dose-response determinations is the isothermal decay method. In such an experiment, a sample is

given a fixed amount of radiation, subjected to isothermal heat (constant temperature for a given time), and then the luminescence or ESR signal is measured; the experiment is repeated for different combinations of temperatures and holding times, until the nature of thermal decay can be described well by a kinetic model. Fig. 2J–L shows the isothermal decay data obtained using the same protocols as for the dose

response data in the panel above, and subject to the same quality control criteria. The thermal kinetic parameters can be derived by fitting the laboratory data with a kinetic model and a range of different models have been proposed for this purpose. Quartz OSL often exhibits first-order isothermal loss (e.g. Wintle and Murray, 2006) which can be entirely described through an Arrhenius law (Eq. 2). In contrast, the thermal depletions of quartz TL/ESR or feldspar OSL are considerably more complicated, and involve high-order kinetics (e.g. Toyoda and Ikeya, 1991; Prokein and Wagner, 1994; Guralnik et al., 2015c), or alternatively, multi-exponential models (e.g. Poolton et al., 2009; Li and Li, 2013; Jain et al., 2015; Guralnik et al., 2015c; King et al., 2016a).

In minerals in which anomalous fading is ubiquitous (e.g. feldspar, or volcanic quartz), this rate of athermal loss must be quantified on equal terms with isothermal decay. Practically, the measurement of samplespecific anomalous fading rates often reduces to an isothermal storage experiment at room temperature (Aitken, 1985; Lamothe and Auclair, 1999; Auclair et al., 2003). Fading experiments monitor luminescence intensity decay with time, and can be described by a range of different models (e.g., Huntley and Lamothe, 2001; Lamothe et al., 2003; Huntley, 2006) all centred around the concept of quantum mechanical tunnelling of trapped electrons to their nearest neighbouring holes, Fig. 2L shows the anomalous fading of Na-feldspar IRSL at 15 °C, greatly exceeding the zero thermal loss predicted from extrapolation of higher-temperature data. This effect, first described in feldspars by Garlick and Robinson (1972), can result in age underestimation if unaccounted for (Huntley and Lamothe, 2001), although recent adaptations to feldspar luminescence measurement protocols (Li and Li, 2011a; Buylaert et al., 2012) can target feldspar OSL sub-signals with much less to negligible fading.

3.4. Environmental dose rate determination

The sample-specific environmental dose rate (\dot{D} in Eq. 2) can be constrained through direct counting of alpha, beta and gamma decays, or via geochemical measurement of radioactive element concentrations (i.e. U, Th, K and Rb; Aitken, 1985) in the host rock, as well as within the target mineral grains (e.g. internal K-content in feldspar). For the latter approach, radiation dose rates are calculated using conversion factors derived from nuclear data tables (e.g. Guerin et al., 2011). The calculated dose rates are then adjusted for attenuation caused by mineral shape and grain-size, as well as water content and alpha efficiency (see Durcan et al., 2015 and references therein). For shallow samples taken at the immediate surface of the Earth, a cosmic-ray component (\sim 0.1–0.3 Gy ka⁻¹) may also contribute to the total dose rate, especially in mafic lithologies with low abundances of radioisotopes ($\dot{D} \sim 1$ –3 Gy ka⁻¹, e.g. Tsukamoto et al., 2010, 2011).

Within thermochronometry applications, the environmental dose rate can be a major source of uncertainty, due to the challenge of estimating the pre-crushed quartz or feldspar grain size, and potential contribution of signal from inclusions (Sohbati et al., 2013; King et al., 2016a). However, in contrast, thermometry applications are relatively unaffected because the environmental dose rate exerts only a logarithmic control on the derived palaeotemperature (Eq. (A.10b) in Guralnik et al., 2013). To overcome such \dot{D} uncertainties, grain sizes should be routinely estimated from examination of thin-sections of the bedrock parent material, and the mineralogical composition of the aliquots further quantified to the best possible level.

3.5. Age determination

In its simplest form, trapped-charge age is given by dividing the equivalent dose received in nature, D_e , by the estimated dose rate, \dot{D} (Aitken, 1985). However a more rigorous approach is required to calculate ages when the dose rate is not constant with time (e.g. Tsukamoto et al., 2014), or when signal losses are involved (see Kars et al., 2008 for treatment of athermal loss correction, and Liu et al., 2016 for thermal loss correction). In the latter approaches, the \dot{D} term remains constant,

but the equivalent dose D_e is functionally replaced by a combination of n/N (fraction of saturation), D_0 (the characteristic dose), and possibly other terms (e.g. kinetic order, residual dose).

In the most general scenario, an observed natural fraction of saturation $(n/N)_{nat}$ may be converted into an apparent age t_{app} via numerical solution of the governing differential equations (e.g. Eqs. (1) and (3), or variations thereof), given a prescribed temperature (typically constant), and potentially other time-dependent terms. To propagate all uncertainties, Monte-Carlo simulations with randomized kinetic parameters can be used (e.g. Guralnik et al., 2015a). To find which thermal histories might have led to the observed t_{app} , the governing differential equations are solved once again, but this time with pre-defined (or totally random) time-temperature histories. The difference between the observed, and thermally-modelled ages may be evaluated using standard methods such as the chi-square statistic (Guralnik et al., 2015a) or a classical rejection algorithm (see King et al., 2016a and references therein).

4. Limitations

4.1. Signal saturation: thresholds and limits

The saturation of trapped-charge systems at 10^{5-6} years is one of the biggest challenges and limitations to their use in thermochronometry. The evolution of apparent age and trapped-charge concentration for different cooling rates (and a final cooling temperature of 0 °C), is shown in Fig. 3 for two recently-investigated OSL thermochronometers (see Fig. 3 caption and Table 2 for kinetic values). Notably, both systems reach field saturation at ≤ 400 °C Ma $^{-1}$, and would only be applicable at cooling rates exceeding ~ 400 °C Ma $^{-1}$. Comparing the growth of trapped electrons for the 10 °C Ma $^{-1}$ cooling rate in Fig. 3B and D, one can note that in the case of quartz OSL, virtually all traps are eventually populated with electrons in nature, while in feldspar OSL, a noticeable subset of traps remains empty even at very long irradiation times, due to a competing athermal signal loss.

Wintle and Murray (2006) proposed a threshold for finite quartz OSL ages of $n/N \sim 85\%$, due to the increasing uncertainty of interpolating the natural trapped-charge population ('Nat.', Fig. 2) onto the saturating part of the dose response curve $\sim 15\%$ away from full trap saturation. Guralnik et al. (2015b) extended this threshold to systems that may have experienced signal loss (due to elevated temperature, anomalous fading, or a combination thereof), to "15% below field saturation level $(n/N)_{ss}$ " (grey areas in Fig. 3B,D). Although this value is somewhat arbitrary, it was chosen to reflect a cautious and conservative assessment of uncertainties in the signal saturation zone. As our understanding, measurement and description of trap saturation improves, it may be that this threshold will reduce, extending the application of trapped-charge methods to older ages and hence slower cooling rates.

Notice that although in Fig. 3D, all cooling histories evolve to n/N < 0.85, the three slowest cooling scenarios terminate within 15% of the predicted trap occupancy at field saturation $(n/N_{ss} = 0.76)$, hence implying that the resultant OSL signals can be inverted to minimum ages and maximum cooling rates only. The lower detection limits of typical TL, ESR and OSL signals in thermochronometry are listed in Table 2 (calculated following first-order approximation via Eqs. (1)-(2)). Most notably, while TL and OSL seem to be restricted to extremely rapid cooling scenarios (>100 °C Ma $^{-1}$), ESR exhibits the latest saturation and thus offers the potential for constraining slower cooling rates (in the >10 °C Ma $^{-1}$ range).

As noted by Li and Li (2012), saturation effects of trapped-charge chronometers at slow cooling rates may invalidate the classical approach of closure temperature calculation, developed for systems with infinite storage space (Dodson, 1973; Herman et al., 2010). Given that closure temperature is often used in thermochronometry, relating the apparent age of the sample to its corresponding palaeotemperature (for a given cooling rate), a modified calculation scheme for saturating

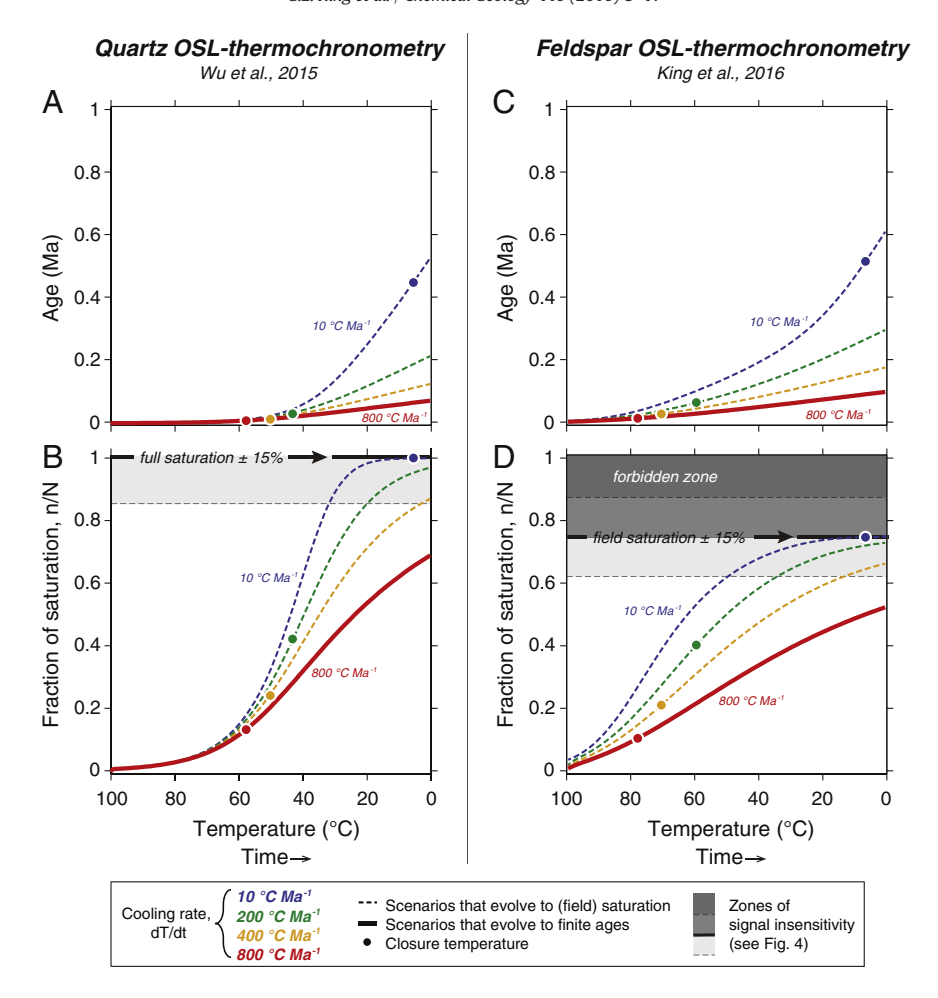


Fig. 3. Limits of OSL-thermochronometry. OSL age (A, C) and signal (B, D) accumulation for different rates of cooling for quartz and feldspar, respectively. Solid lines show scenarios where finite ages can be derived, whereas dashed lines show scenarios that result in ages that cannot be differentiated from field saturation values. Quartz OSL does not suffer from anomalous fading, and therefore field saturation values of n/N = 1 may be reached at slow cooling rates (B). In contrast, feldspar OSL is affected by athermal signal loss, and the field saturation is n/N = 1 may be reached at slow cooling rates (B). In contrast, feldspar OSL is affected by athermal signal loss, and the field saturation is n/N = 1 may be reached at slow cooling rates (B). In contrast, feldspar OSL is affected by athermal signal loss, and the field saturation is n/N = 1. Kinetic parameters for the two systems are listed in Table 2; additional parameters (not tabulated) include general order of $\beta = 1.88$ for quartz OSL (Wu et al., 2015), and athermal stability parameters $\bar{s} = 10^{15.48}$ s⁻¹ and $\rho' = 10^{-5.95}$ for feldspar OSL (King et al., 2016a). Both signals become distinguishable from (field) saturation only at cooling rates exceeding 400 °C Ma⁻¹.

systems has been devised (Guralnik et al., 2013) which, for a first-order system is given by:

$$T_{c}(T_{0}, T_{P}) = \left\{ \frac{1}{T_{P}} - \frac{k_{B}/E}{\tau \lambda - \tau K_{p}} \ln \left[1 + \frac{\tau \lambda - \tau K_{p}}{(\tau K_{p})^{\tau \lambda} e^{-\tau K_{p}}} (\Gamma(\tau \lambda, \tau K_{p}) - \Gamma(\tau \lambda, \tau K_{0})) \right] \right\}^{-1}$$

$$(4)$$

where τ is the cooling time constant (Ma), T_0 and T_P the initial and final temperatures of cooling (K), K_0 and K_P are shorthand for $s \exp(-E/k_BT_0)$ and $s \exp(-E/k_BT_P)$, $\lambda = -\dot{D}/D_0$ the electron trapping rate (Ma⁻¹), and $\Gamma(a,z)$ the upper incomplete gamma function. For the general case of non-first-order systems, closure temperatures can be calculated numerically (Eq. (5) in Guralnik et al., 2013). Such numerically-obtained closure temperatures (assuming first-order kinetics, but linear cooling rates) are shown in Fig. 3 as filled circles of corresponding colour. Apart from the familiar trend of increasing closure temperature at faster cooling rates, one particularly notable feature in Fig. 3 is that some T_C values clearly do not correspond to the onset of signal growth. This is most pronounced for the 10 °C Ma⁻¹ scenario, for which notable electron trapping commences at ~60 °C (quartz OSL) and ~80 °C (feldspar OSL), yet the $T_{C,10}$ of both systems is ~5 °C. Such asymptotic merging of T_C towards the final temperature of cooling (Guralnik et al., 2013) is due to the fact, that at progressively slow cooling rates, the apparent ages of both systems reach their limiting values of ~0.5 Ma. Thus, while product accumulation may have commenced ~6–8 Ma before present, these systems fundamentally cannot retain any thermal information beyond their apparent ages of ~0.5 Ma (Guralnik et al., 2013). The above example highlights the fact, that while conventionally closure temperatures are reported for a baseline cooling rate of 10 °C Ma⁻¹, such values may be uninformative for trapped-charge thermochronometers, which often saturate at such cooling rates. The easiest compromise seems to be to report the closure temperature of the minimum detectable cooling rate (e.g. Wu et al., 2015; Guralnik et al., 2015a).

4.2. Anomalous fading: screening for thermal signals

For minerals such as feldspar, which are affected by anomalous fading, the measured trapped-charge population will be significantly smaller than for a non-fading mineral, given an identical thermal history. If this effect is not corrected for, samples which are in field saturation (i.e. in an equilibrium between charge trapping and athermal detrapping) may be erroneously inverted into "artefact cooling rates", which simply mistake athermal losses for thermal losses. Following the theoretical developments of Huntley (2006) and Kars et al. (2008), athermal steady-state (i.e. the point at which charge trapping is equal to charge detrapping due to anomalous fading) can be evaluated for a given sample providing that its \dot{D} , D_0 and fading rate are known (Fig. 4). Furthermore, both the observed natural luminescence intensity and the laboratory

maximum intensity are affected by fading, and a correction is thus needed to obtain the relative trap occupation (Guralnik et al., 2015a; King et al., 2016a; Valla et al., 2016), which can then be compared to the athermal steady-state prediction. Where the measured and predicted fractions of saturation are equal, the sample is considered to be in field steady-state, and can only provide the minimum rate of cooling or a maximum palaeotemperature (e.g. the five shallowest samples in Fig. 4A).

4.3. Measurement uncertainties

The majority of trapped-charge dating applications are focussed on constraining the chronologies of sedimentary archives. The relatively slow rate of optical signal bleaching of the Al and Ti ESR centres (e.g.

Yokoyama et al., 1985; Walther and Zilles, 1994), has limited the application of ESR in sedimentary settings, where OSL is frequently utilised. Consequently, despite its potential for extending the age range over which Quaternary sedimentary histories can be constrained, ESR dating has not benefitted from the same intensive development that followed the introduction of the SAR protocol in luminescence dating >15 years ago (Murray and Wintle, 2000). Fully automated ESR instruments have not yet been developed, and for practical reasons the majority of quartz ESR measurements comprise multiple-aliquot protocols, which have inherently greater uncertainties. A multiple-aliquot method comprises the irradiation of multiple sub-samples to develop a single dose-response curve, from which the trapped-charge concentration can be interpolated (cf. Appendix A, Rink, 1997). Intra-aliquot variance

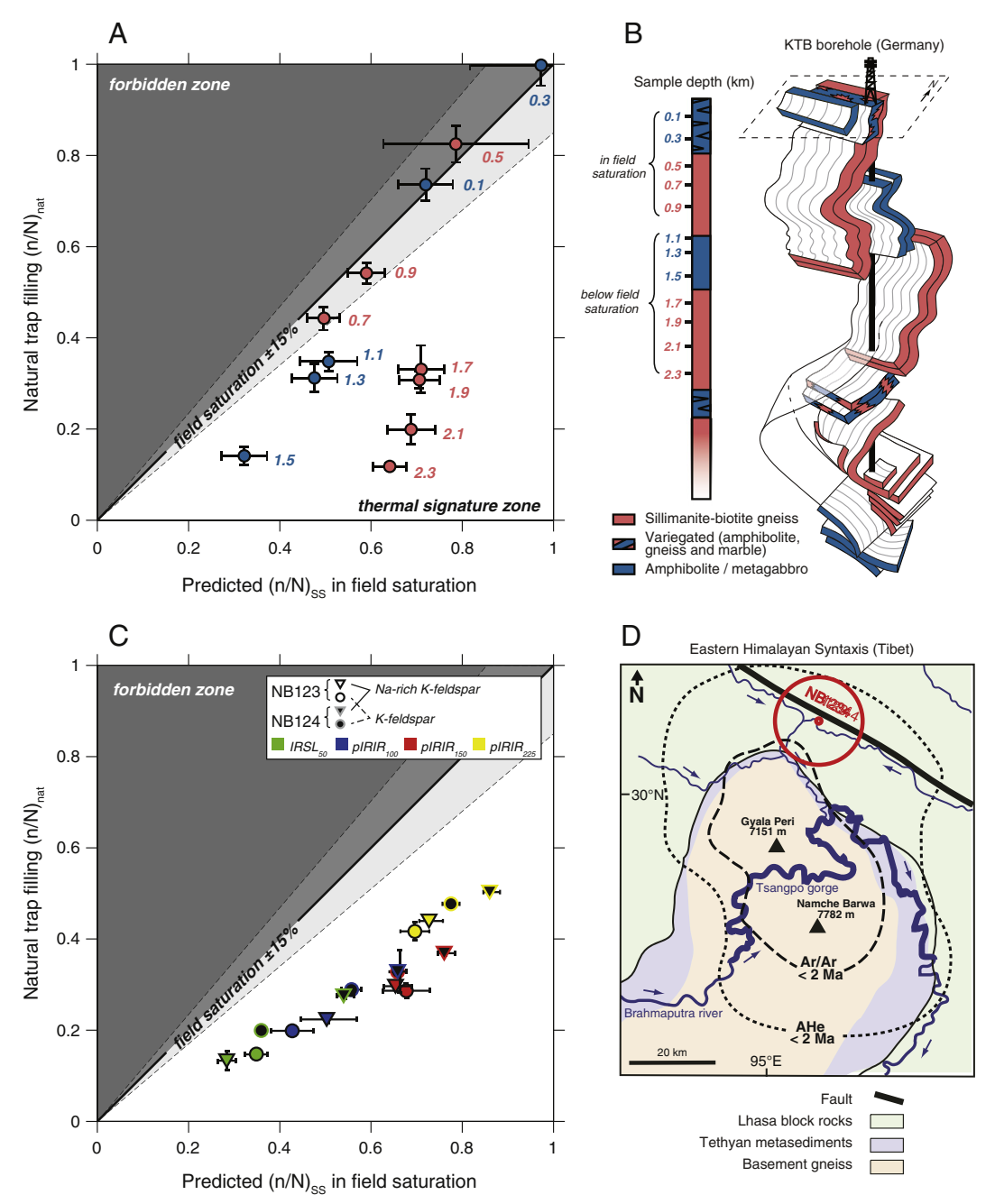


Fig. 4. Screening of feldspar OSL data for a thermal signal. Predicted athermal steady-state values, $(n/N)_{SS}$, are contrasted with measured natural trap filling values, $(n/N)_{nat}$ for samples from a thermal steady-state (A–B) (Guralnik et al., 2015a) and an actively cooling setting (C–D) (King et al., 2016a). Athermal signal losses mean that a fraction of saturation of $(n/N)_{nat} < 1$ may not necessarily relate to thermal losses. Such is the case with the five shallowest borehole samples at the KTB-borehole (A), in which $(n/N)_{nat} \sim (n/N)_{SS}$; yet only below 1 km depth, do the samples exhibit detectable thermal signatures (irrespective of lithology). In contrast, the two samples from the Namche Barwa massif (Eastern Himalayan syntaxis, Tibet) experience extremely rapid cooling throughout exhumation, resulting in $(n/N)_{nat} < (n/N)_{SS}$ for all IRSL signals from both samples (King et al., 2016a).

can result in a relative reduction in precision (e.g. Grün et al., 1999), and very large sample masses are required (g rather than mg). However, recently an irradiation and heating unit specific for ESR samples has been developed (Oppermann and Tsukamoto, 2015), facilitating single-aliquot quartz ESR dating (Tsukamoto et al., 2015); furthermore, single-grain ESR measurements have also recently been proposed (Beerten and Stesmans, 2006). Such advances will improve the precision and accuracy of quartz ESR investigations, which because of its later signal saturation relative to luminescence methods (Table 2), has enormous potential for thermochronometric studies.

The intensity of luminescence and ESR signals from quartz and feld-spar minerals of the same provenance can vary by many orders of magnitude, although the causes of this variability are not well known. A major source of uncertainty in luminescence studies relates to signal counting statistics, and therefore poor luminescence sensitivity can result in imprecise determinations of the fraction of saturation or equivalent dose value. Alternative sources of error related to trapped-charge measurements (rather than to the environmental dose rate) are derived from instrument reproducibility, beta or gamma-source calibration, interpolation onto the dose response curve and intrinsic behavioural differences between grains (Thomsen et al., 2005).

5. Applications

5.1. TL thermochronometry

Mentioned in passing by Daniels et al. (1953), trapped-charge thermochronometry was first treated theoretically and experimentally in a landmark paper by Houtermans et al. (1957), focused on palaeothermometry of both geological and meteorite samples in the 100–300 °C range. Inspired by this pioneering work, a series of environmental thermometry studies ensued (Zeller and Ronca, 1963; Ronca, 1964; Ronca and Zeller, 1965; Zeller, 1968), where TL signals were used to reconstruct palaeothermometric conditions in Antarctica and elsewhere. While their inferred timing of Antarctic glaciation (<2 Ma) clearly underestimates currently accepted values by over an order of magnitude, their methods were certainly pioneering, and the mismatch is easily explained by their measurement of bulk rock samples rather than individual minerals, as done today. Most importantly, these studies established the fundamental analytical approaches used in trapped-charge thermochronometry today, including dose response and isothermal decay experiments (see Fig. 2G,J), extrapolation of laboratory high-temperature behaviour into environmental temperatures, and quantification of the trade-off between apparent age and apparent temperature (see Guralnik et al., 2013 and references therein).

During the peak of NASA's Apollo program, the approaches developed by Zeller's group were replicated and applied to thermometry of lunar material. Dalrymple and Doell (1970) were the first to note that "TL observed in a near-surface sample is probably the result of a dynamic equilibrium between the growth of TL due to radiation and its decay in the lunar thermal environment". Based on an analytical foundation for reconstructing environmental temperatures (Christodoulides et al., 1971), Hoyt et al. (1971) and Walker et al. (1972) were able to infer a thermal gradient of $2\pm 2~{\rm ^{\circ}C}~{\rm km}^{-1}$ in a lunar soil, coincident with independent estimates. Later detailed studies enabled further constraint of the lunar surface palaeotemperature both in sunlit (~70–90 °C; Durrani et al., 1972, 1973) and shaded areas (~— 20 °C; Durrani et al., 1977).

Following the successful application of TL thermometry during the lunar exploration era, TL thermometry was developed within the context of geothermal and hydrocarbon exploration in the late 1970s to 1980s. Comparing young TL ages of volcanic bedrock quartz against older apatite fission-track ages obtained from the same lithologies, Takashima (1979, 1985) attributed the age discordance to hydrothermal alteration events. After only a few years, TL was first patented (Hochman and Ypma, 1988, 1990) and then used in the scope of

hydrocarbon maturation assessment (Ypma and Hochman, 1991), in combination with fission-track and vitrinite reflectance data. Unfortunately, the core assumption of the method (a continuum of trap depths which enables the position of the dominant quartz TL peak to be related to the environmental palaeotemperature) remained underexplored, and although still promising, we are unaware of the method's current use in applied geoscience.

Shifting the focus back to theoretical rather than applied geoscience, Tsuchiya and Fujino (2000) reported ESR and TL data for the Takidani Pluton in the Japanese Alps, inferring a TL closure temperature of ~70 °C and interpreting their TL ages (91–152 ka) as markers of an abrupt change in the pluton's cooling history. Two more recent contributions to TL thermochronometry include that of Gong et al. (2010), who obtained quartz TL ages from boreholes in Eastern China and qualitatively inferred recent exhumation for parts of their corresponding sedimentary basins (Fig. 5A), and Schmidt et al. (2015), who demonstrated a decrease of quartz red TL intensity in a drillhole in the granitic basement of Southern Germany.

5.2. ESR thermochronometry

Ikeya (1983) attributed the departure of an ESR centre concentration from its projected thermal equilibrium value to a recent influx of cold water in a subsurface aguifer (~0.6 km depth) in the vicinity of the Hachobara geothermal power station in Japan. Some years later, Toyoda and Ikeya (1991) proposed that the intensity of various ESR centres in bedrock quartz can be used to determine the low-temperature thermal histories of their host rocks. Using for the first time the concept of 'closure temperature' (Dodson, 1973) in the context of trappedcharge dating, they determined T_{C,10} of 91 °C (E' centre), 78 °C (Ti centre), and 31 °C (Al centre). While initial attempts to quantify cooling rates using ESR resulted in either circular or inconclusive arguments (Agel et al., 1991a, 1991b; Scherer et al., 1993; see discussion in Grün et al., 1999), the first comprehensive ESR thermochronometry applications concerned the Eldzhurtinsky Granite drillholes in the Russian Caucasus (Koshchug and Solovyov, 1998; Grün et al., 1999). By extrapolating the non-linear thermal behaviour of ESR to low temperatures, Grün et al. (1999) obtained kinetic parameters that corresponded to a closure temperature of $T_{C,10}$ ~55 °C (Ti centre) and ~49 °C (Al centre). The age-depth profiles of each ESR centre from the two boreholes exhibited diminishing age with depth (see their upper core data redrawn in Fig. 5B), and was further interpreted as indicating differential cooling rates for the lower (600 °C Ma⁻¹) and upper (200 °C Ma⁻¹) borehole as the result of Quaternary valley carving.

5.3. OSL thermochronometry

Noting that the exceptionally low closure temperature of luminescence thermochronometers offers great potential for quantifying latestage rock exhumation, Herman et al. (2010) introduced OSL thermochronometry to constrain late-stage exhumation rates in the Southern Alps of New Zealand. The use of OSL, rather than TL or ESR, enabled for the first time advantage to be taken of the most-widely used trapped-charge dating method (Roberts and Lian, 2015). Herman et al. (2010) reported quartz OSL ages in the range of 14-155 ka, which were inverted into cooling rates of ~300 °C Ma⁻¹, and associated erosion rates of ~ 8 mm a⁻¹. These results suggested that over a ~ 0.1 Ma timescale, regional exhumation rates remained similar to those recorded by higher-temperature thermochronometric techniques over longer timescales (1–10 Ma), reinforcing the idea of constant exhumation leading to topographic steady-state in the Southern Alps. Shortly after, De Sarkar et al. (2013) applied the same methodology in combination with apatite fission-track (AFT) and ⁴⁰Ar-³⁹Ar dating in the Western Arunachal Himalaya (India). Using a double-SAR protocol (Roberts, 2007) to address the contamination of quartz by feldspar, they obtained ages of 10-30 ka which correlated well with the samples' elevation

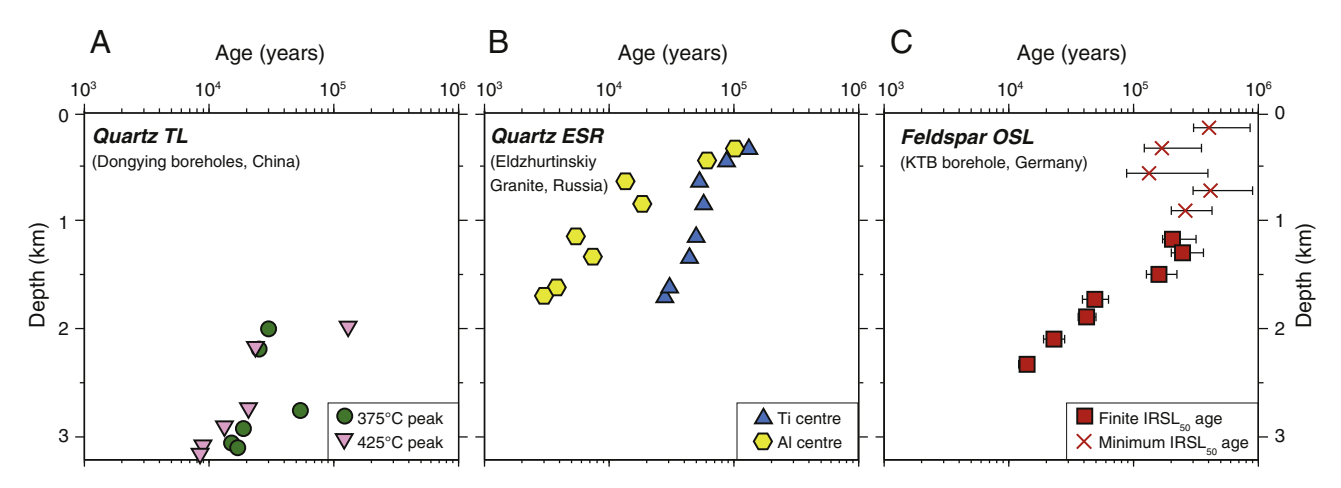


Fig. 5. Palaeo-thermometry and thermochronometry applications using trapped-charge methods. (A) Using two different quartz TL emission peaks (cf. Fig. 2D), Gong et al. (2010) were able to calculate equivalent temperatures from their luminescence ages, which were in agreement with independent temperature controls, within the Dongying sedimentary basin, China. (B) Using the Ti and Al ESR centres, Grün et al. (1999) were able to measure cooling rates of $160-600\,^{\circ}\text{C}$ Ma $^{-1}$ for the Eldzhurtinskiy granite, Caucasus, concluding that ESR measurements of paramagnetic quartz centres will enable the reconstruction of landscape dynamics over $10-1000\,$ ka timescales. (C) Using the IRSL $_{50}$ signal of Na-feldspar, Guralnik et al. (2015a) were able to validate the application OSL-thermometry within the well-studied KTB-borehole, Germany, which has been thermally stable for ~25 Ma (Coyle et al., 1997). Whilst the IRSL $_{50}$ Na-feldspar system yielded only minimum ages (or maximum palaeotemperatures) in the topmost 1 km of the borehole, the seven finite ages below could be successfully inverted into a geothermal palaeogradient of $29\pm2\,^{\circ}\text{C}$ km $^{-1}$ in the last ~60 ka.

(1.7–3.7 km asl). De Sarkar et al. (2013) interpreted this age-elevation relationship as evidence for an acceleration of erosion by a factor of ~100 (in comparison to the available higher-temperature AFT and ⁴⁰Ar-³⁹Ar thermochronometric data), the latter result should be treated with caution, given that such direct conversions of age-elevation data into exhumation rates are often biased (see Braun, 2002).

Two shortcomings of these early applications have been highlighted subsequently, comprising: (i) a lack of characterisation of signal saturation effects (Li and Li, 2012; Guralnik et al., 2013), and (ii) a common contamination of the OSL signal in bedrock quartz by feldspar emissions (Guralnik et al., 2015b). While point (i) meant that the originally presumed $T_{C,10}$ of 30–35 °C for quartz OSL (Herman et al., 2010) was optimistic (as the system saturates even at 100 °C Ma⁻¹; Guralnik et al., 2013), point (ii) implied that even a theoretically accessible T_{C200} of ~50 °C would be difficult to obtain in practice, due to the problematic nature of quartz OSL signals in most bedrock quartzes of high-grade metamorphic or magmatic origin. Following the above considerations, Wu et al. (2015) presented a detailed assessment of four meta-sandstone quartz samples from the Hsuehshan Range (Taiwan), demonstrating acceptable quartz OSL behaviour in low-metamorphic metasediments, and inferring that the minimum cooling rate that quartz OSL could be used to detect is 360 ± 100 °C Ma⁻¹, with a corresponding T_{C360} of 44 \pm 7 °C.

Another study, which tested an experimental OSL protocol (Ankjærgaard et al., 2015) on palaeosols interbedded between volcanic layers from the Golan Plateau (Israel), found that the lowest accessible cooling rate would be ~2 °C Ma $^{-1}$, with an associated $T_{\rm C.2}$ of ~40 °C ($T_{\rm C.10}$ of ~70 °C). However, this study documented severe (60–80%) OSL age underestimations relative to their bracketing K-Ar chronology (in the 1.6–0.8 Ma range). Since the cooling rates required to explain the OSL ages were unrealistic (>4000 °C Ma $^{-1}$), the origin of the discrepancy was attributed either to expected geothermal anomalies (e.g. extinct hotsprings in the ~80 °C range), unresolved methodological problems, or most likely a combination of both.

To overcome the challenge of quartz OSL contamination by feldspar emissions, the target mineral for OSL thermochronometry has been reconsidered and feldspar determined as a viable alternative using IRSL. Guralnik et al. (2015a) presented a study from the German Continental Deep Drilling Borehole, demonstrating a decrease of Na-feldspar IRSL ages with depth (Fig. 5C), and inverting them into a geothermal palaeogradient of 29 ± 2 °C km $^{-1}$ over an unprecedented ~60 ka timescale. Further characterisation of the Na-feldspar OSL system resulted in positioning of its partial retention zone in the 40–65 °C range, and

estimation of its lowest accessible closure temperature as $T_{C,190} = 53$ °C. This study was the first direct validation of OSL thermometry in a well-known and well-studied continental subsurface environment, whose thermal history has been constrained by a multitude of other independent methods.

Following this borehole validation study, further investigations were carried out to find feldspar OSL signals that could be used to record rapid exhumation of deep-seated rocks towards the Earth's surface. Valla et al. (2016) presented a large dataset of feldspar OSL from 32 bedrock samples from Alaska and Norway, out of which only signals from the fastest exhuming location (Yakutat Terrain in Alaska; ~1-3 km Ma⁻¹; Enkelmann et al., 2015) were significantly below field saturation. Focusing further research on similarly extreme settings, King et al. (2016b) explored one of the most rapidly (>5 km Ma⁻¹; Zeitler et al., 2014) exhuming settings on Earth (Namche Barwa, Himalaya), and investigated the potential of multi-OSL-thermochronometry (King et al., 2016a). Trapped-charge thermochronometry presents a great collection of various electron traps with a range of thermal stabilities in the 1-2 eV range (Table 2), thus it offers the potential for measuring multiple signals from a single rock sample, both from different minerals within the rock but also different traps within a given mineral (e.g. Grün et al., 1999; Gong et al., 2010; Qin et al., 2015; King et al., 2016a). Where the signals are inverted together, continuous cooling histories can be obtained, as illustrated in Fig. 6 where the results of a single-system and multi-system inversion are contrasted. Whereas using only the IRSL50 signal of K-feldspar is able to constrain a cooling history of ~750 °C Ma⁻¹ over ~0.05 Ma (Fig. 6A-B), using multiple IRSL signals enables this cooling history to be constrained over the past ~0.1 Ma (Fig. 6C-D). Multi-luminescence (or other trapped-charge) thermochronometric methods also offer an improvement in precision relative to single-system approaches. King et al. (2016b) used a multisignal approach to measure eight samples from the Namche Barwa massif, Tibet, eastern Himalaya. Whilst three samples had infinite ages related to relatively slow rates of rock cooling ($\leq 200 \, ^{\circ}\text{C Ma}^{-1}$), the five remaining samples produced finite ages, corresponding to cooling rates of ~300-1500 °C Ma⁻¹. Using a 1D thermal model, the OSLthermochronometry data were contrasted with thermochronometric data, revealing an acceleration in exhumation rate in the past ~1 Ma at the northern end of the Namche Barwa dome. King et al. (2016b) related this change in exhumation rate to continued northward migration of the dome, and associated capture of the Parlung river.

6. Outlook

6.1. Signal saturation and alternative mineral-signal pairs

A major drawback of trapped-charge dating in general and thermochronometry in particular, is signal saturation, which limits the applicable dating, and hence cooling rate range. For many signals, the saturation limits are presently not well constrained (e.g. for the different ESR signals), furthermore for feldspar IRSL signals, saturation levels are dependent on the presence of athermal loss, which must be quantified in the laboratory. Therefore, as for geochronometry, a quest remains for trapped-charge signals that grow to higher doses, and which can be well constrained through laboratory measurement.

A range of recently identified luminescence signals offer this potential, including a thermally-transferred OSL signal, and a violet stimulated luminescence signal (VSL), both of which have been measured in quartz (Wang et al., 2006; Jain, 2009; Ankjærgaard et al., 2013). A TL emission from quartz, detected in the red part of the visible spectrum, has also been observed to saturate later than other quartz signals (Schmidt et al., 2015 and references therein). For feldspars, increased temperature IRSL measurements (i.e. at temperatures >100 °C) result in more athermally stable signals (Thomsen et al., 2008; Buylaert et al., 2009; Li and Li, 2011a; Li and Li, 2011b), for which the determination of saturation is less dependent on anomalous fading. However, the VSL and high-temperature IRSL signals also exhibit increased thermal stability (Li and Li, 2012; Ankjærgaard et al., 2013), which results in earlier

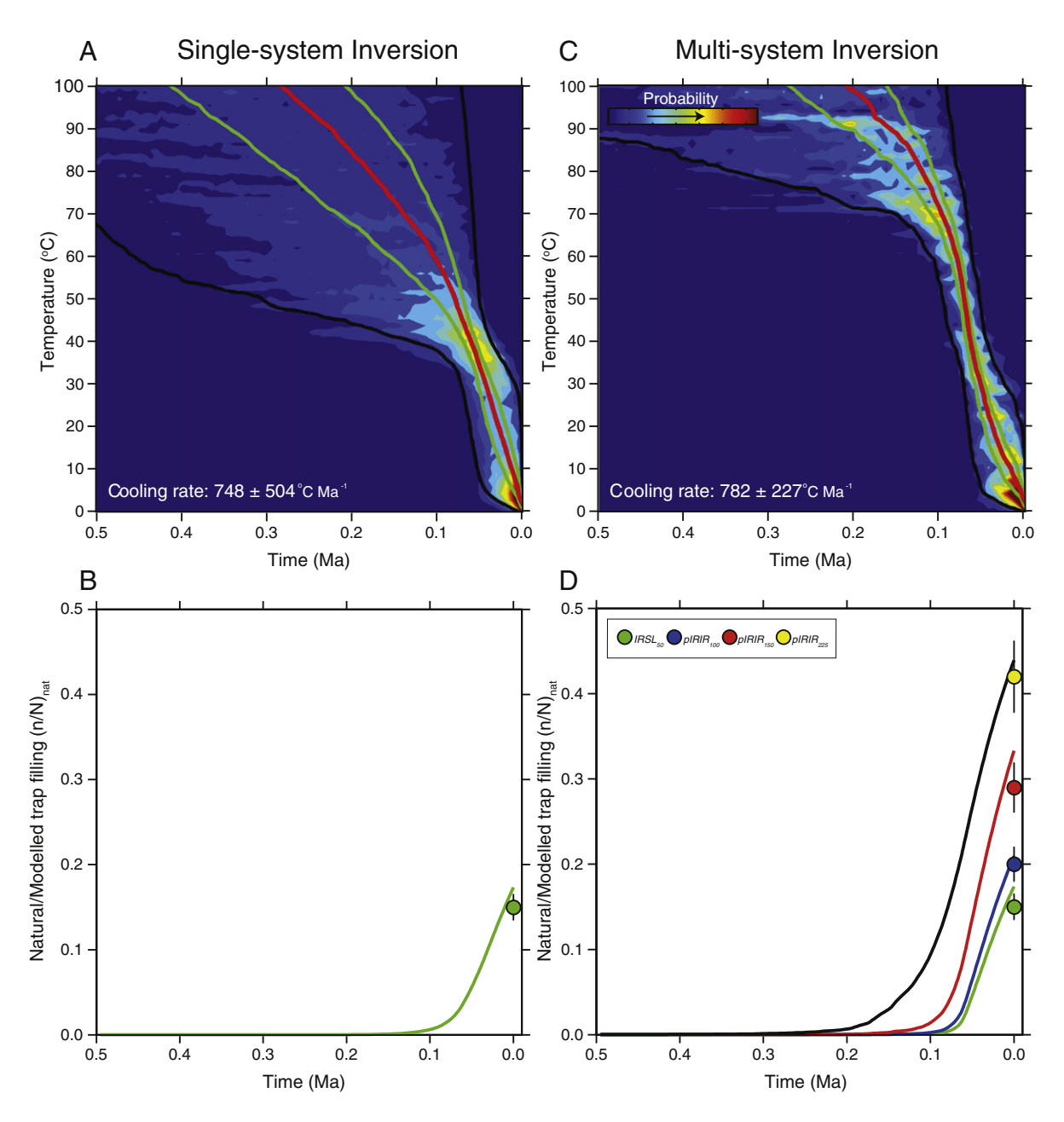


Fig. 6. Comparison of cooling histories derived from single and multi-system inversions of OSL-thermochronometry data. (A) Inversion of the IRSL₅₀ signal measured from K-feldspar extracted for sample UNIL/NB123 from Namche Barwa, Tibet (King et al., 2016a). A Monte-Carlo search of different time-temperature histories between 150 °C and 5 ± 5 °C, over 0.5 Ma was done. The resultant values from different modelled time-temperature histories were then accepted or rejected according to a rejection algorithm (von Neumann, 1951). The black and green lines are the 95% and 68% confidence intervals respectively, and the red line is the median model; shading reflects likelihood score. In (B) the dose response curve for the median model is plotted relative to the measured $(n/N)_{nat}$ value. (C) Inversion of the IRSL₅₀, post-IR IRSL₁₀₀, post-IR IRSL₂₂₅ signals measured for the same sample using a MET measurement protocol (King et al., 2016a), using the same inversion method. A more precise cooling history is obtained which extends over a longer time period than from using a single system. (D) Contrasts the modelled dose response of the different signals calculated for the median model, relative to the measured $(n/N)_{nat}$ values.

signal accumulation thus counteracting their later onset of saturation. Whilst the luminescence signals of quartz and feldspar certainly warrant further investigation, it may be that the luminescence signals of other minerals will contribute significantly to the development and application of trapped-charge thermochronometry. For example, the establishment of self-consistent dosimetric protocols for the TL of biogenic carbonates, which saturate later than most quartz and feldspar luminescence signals (Duller, 2015b and references therein; Duller et al., 2015), have an attractive range of thermal stabilities (Stirling et al., 2012 and references therein) and are thus highly encouraging for potential low-temperature thermochronometry of carbonate terranes.

Different minerals and different signals will require the improvement of existing and development of new kinetic models to constrain charge trapping and detrapping behaviour. These processes may sometimes be described equally well by different models, both on laboratory and geological timescales (e.g. Guralnik et al., 2015c). For example, the origin of IRSL from feldspar is subject to an ongoing debate regarding whether all luminescence emissions can be explained by a single, or multiple-trap model (cf. Andersen et al., 2012; Jain et al., 2012; Pagonis et al., 2014), which affects both simulated signal growth and decay, as well as our confidence in differentiating and extracting particular trap (sub)populations. In even more challenging cases, only qualilinks between luminescence sensitivity and palaeotemperature have so far been established (Liu et al., 2015); mathematical models have yet to be devised for this potentially important and useful phenomenon. Since selection of appropriate models is central for correct interpretation of thermal histories of rocks (e.g. Wauschkuhn et al., 2015; Shuster et al., 2006; Gautheron et al., 2013), trapping model evaluation and verification remain among the key research challenges for the future development of trapped-charge thermochronometry. Once established, such models will need to be implemented into thermo-kinematic models to enable interpretation of the data in terms of landscape evolution. Current efforts are underway to incorporate models for quartz and feldspar into common thermochronological software, including Pecube (Braun, 2003; Braun et al., 2012) and QTQt (Gallagher, 2012).

6.2. Alternative uses: characterisation of radiation damage

Characterising and quantifying the degree of radiation damage is a key question for thermochronometric methods such as (U-Th)/He of zircon or apatite, because of the effects that radiation damage has on the retention of radiation daughter products (e.g. Guenthner et al., 2014; Djimbi et al., 2015). The luminescence sensitivity and emission spectrum of quartz is extremely sensitive to its radiation history (e.g. Rink, 1994; King et al., 2011 and references therein), and therefore could provide additional insights into the irradiation history of rock or mineral samples. For example, the intensity of the quartz ESR E' centre has been correlated with the density of alpha tracks (Kohno et al., 1995; Toyoda et al., 2001), and may hence prove to be a useful proxy for radiation damage, if developed further. Both TL and ESR of zircon and apatite could also be utilised as proxies for fission-track density, following recurring mention of an anti-correlation between fission-track density and TL/ESR intensity (Vaz and Senftle, 1971; Shulgin et al., 1974; Durrani et al., 1984; Amin, 1989; Ishii et al., 1991). However at low levels of radiation damage, contrary effects, i.e. generation rather than destruction of luminescent defect centres, may be the dominant process (e.g. Kasuya et al., 1990; Nasdala et al., 2013). Additionally, anomalous fading may be related to the degree of radiation damage in crystals (Durrani and Amin, 1985); both zircon and apatite, wellknown for their relatively high U and Th contents, exhibit strong anomalous fading of luminescence signals (e.g. Templer, 1985; Polymeris et al., 2014). Thus anomalous fading (generally considered as a 'nuisance' in luminescence dating) could become a useful and quantitative proxy for radiation damage in highly radioactive accessory minerals.

7. Conclusions

Trapped-charge thermochronometry is characterised by its extremely low closure temperature, which is presently constrained to ~40–100 °C depending upon the targeted mineral and signal investigated. Although various studies have utilised TL and ESR to investigate rock thermal histories over the past fifty years, OSL thermochronometry has only recently been developed to constrain late-Quaternary landscape evolution (e.g. King et al., 2016b) and for determining subsurface (palaeo)temperature conditions (e.g. Guralnik et al., 2015a). The major limiting factor for the successful application of all trapped-charge thermochronometry systems is signal saturation, however renewed investigations of TL, ESR and OSL signals, and the exploration of alternative minerals and trapped charge signals may enable further extension of their applicability range.

Acknowledgements

This research was funded by Swiss National Science Foundation (SNSF) grant numbers PP00P2-38956 and 200021-127127 awarded to FH, PZ00P2-148191/1 awarded to PGV and Netherlands Organisation for Scientific Research (NWO) VENI grant 863.15.026 awarded to BG. We are grateful to Sumiko Tsukamoto for valuable discussions regarding the ESR technique. Finally, Cecile Gautheron and an anonymous reviewer are thanked for constructive and stimulating reviews that helped to significantly improve this manuscript.

References

Agel, A., Bershov, L.V., Dusausoy, Y., Hafner, S.S., Petrov, I., 1991a. Paramagnetische Defekte in Quarz und deren thermische und radiologische Abhäingigkeit, KTB Rep. 91–1. Kontinentales Tiefbohrprogram der Bundesrepub. Dtsch., Niedersächs. Landesamtf. Bodenforsch, Hannover, pp. 224–238.

Agel, A., Bershov, L.V., Hafner, S.S., Soboleva, S.V., 1991b. Defektstruktur von Quarz: Natürliche Erzeugung und Zerstörung paramagnetische Zentren. Eur. J. Mineral. Beihefte 3–4.

Aitken, M.J., 1985. Thermoluminescence Dating. Academic Press, London 359 pp.

Aitken, M.J., Fleming, S.J., Doell, R.R., Tanguy, J.C., 1968. Thermoluminescent study of lavas from Mt. Etna and other historic flows: preliminary results. Thermoluminescence of Geological Materials. Academic Press, London and New York, pp. 359–366.

Akber, R.A., Prescott, J.R., 1985. Thermoluminescence in some feldspars: early results from studies of spectra. Nucl. Tracks Radiat. Meas. 10 (4–6), 575–580.

Amidon, W.H., Hobbs, D., Hynek, S.A., 2015. Retention of cosmogenic ³He in calcite. Quat. Geochronol. 27, 172–184.

Amin, Y.M., 1989. A study of the effect of natural radiation damage in a zircon crystal using thermoluminescence, fission track etching and X-ray diffraction. Nucl. Instrum. Methods Phys. Res. Sect. A 280, 314–317.

Andersen, M.T., Jain, M., Tidemand-Lichtenberg, P., 2012. Red-IR stimulated luminescence in K-feldspar: single or multiple trap origin? J. Appl. Phys. 112 (4), 043507.

Ankjærgaard, C., Jain, M., Wallinga, J., 2013. Towards dating quaternary sediments using the quartz violet stimulated luminescence (VSL) signal. Quat. Geochronol. 18, 20, 100.

Ankjærgaard, C., Guralnik, B., Porat, N., Heimann, A., Jain, M., Wallinga, J., 2015. Violet stimulated luminescence: geo-or thermochronometer? Radiat. Meas. 81, 78–84.

Auclair, M., Lamothe, M., Huot, S., 2003. Measurement of anomalous fading for feldspar IRSL using SAR. Radiat. Meas. 37 (4–5), 487–492.

Bailiff, I., 2015. Luminescence, pottery and bricks. Encyclopedia of Scientific Dating Methods, pp. 481–485.

Bateman, M.D., Swift, D.A., Piotrowski, J.A., Sanderson, D.C., 2012. Investigating the effects of glacial shearing of sediment on luminescence. Quat. Geochronol. 10, 230–236.

Beerten, K., Stesmans, A., 2006. The use of Ti centers for estimating burial doses of single quartz grains: a case study from an aeolian deposit similar to 2 Ma old. Radiat. Meas. 41 (4), 418–424.

Blackwell, B.A.B., Skinner, A.R., Blickstein, J.I.B., Montoya, A.C., Florentin, J.A., Baboumian, S.M., Ahmed, I.J., Deely, A.E., 2016. ESR in the 21st century: from buried valleys and deserts to the deep ocean and tectonic uplift. Earth Sci. Rev. 158, 25–159.

Bøtter-Jensen, L., Bullur, E., Duller, G.A.T., Murray, A.S., 2000. Advances in luminescence instrument systems. Radiat. Meas. 32 (5–6), 523–528.

Braun, J., 2002. Quantifying the effect of recent relief changes on age-elevation relationships. Earth Planet. Sci. Lett. 200 (3), 331–343.

Braun, J., 2003. Pecube: a new finite-element code to solve the 3D heat transport equation including the effects of a time-varying, finite amplitude surface topography. Comput. Geosci. 29 (6), 787–794.

Braun, J., Van der Beek, P., Batt, G., 2006. Quantitative Thermochronology: Numerical Methods for the Interpretation of Thermochronological Data. Cambridge University Press

- Braun, J., Van Der Beek, P., Valla, P., Robert, X., Herman, F., Glotzbach, C., Pedersen, V., Perry, C., Simon-Labric, T., Prigent, C., 2012. Quantifying rates of landscape evolution and tectonic processes by thermochronology and numerical modeling of crustal heat transport using PECUBE. Tectonophysics 524, 1–28.
- Brown, K.S., Marean, C.W., Herries, A.I., Jacobs, Z., Tribolo, C., Braun, D., Roberts, D.L., Meyer, M.C., Bernatchez, J., 2009. Fire as an engineering tool of early modern humans. Science 325 (5942), 859–862.
- Buylaert, J.-P., Jain, Mayank, Murray, A.S., Jørkov Thomsen, Kristina, Lapp, Torben, 2012. "IR-RF dating of sand-sized K-feldspar extracts: a test of accuracy.". Radiat. Meas. 47 (9), 759–765.
- Buylaert, J.P., Murray, A.S., Thomsen, K.J., Jain, M., 2009. Testing the potential of an elevated temperature IRSL signal from K-feldspar. Radiat. Meas. 44 (5–6), 560–565.
- Chapot, M.S., Roberts, H.M., Duller, G.A.T., Lai, Z.P., 2012. A comparison of natural- and laboratory-generated dose response curves for quartz optically stimulated luminescence signals from Chinese Loess. Radiat. Meas. 47 (11—12), 1045–1052.
- Chen, R., Pagonis, V., 2011. Thermally and Optically Stimulated Luminescence: A Simulation Approach, John Wiley & Sons 434 pp.
- tion Approach. John Wiley & Sons 434 pp.

 Christodoulides, C., Ettinger, K.V., Fremlin, J.H., 1971. The use of TL glow peaks at equilibrium in the examination of the thermal and radiation history of materials. Mod. Geol. 2. 275–280.
- Coyle, D.A., Wagner, G.A., Hejl, E., Brown, R., Van den Haute, P., 1997. The Cretaceous and younger thermal history of the KTB site (Germany): apatite fission-track data from the Vorbohrung. Geol. Rundsch. 86 (1), 203–209.
- Dalrymple, G.B., Doell, R.R., 1970. Thermoluminescence of lunar samples. Science 167 (3918), 713–715.
- Daniels, F., 1953. Thermoluminescence dosimetry. In Seminar on the Effects of Ionizing Radiations. Evans Signal Corps Engineering Laboratories, Belmar, NJ.
- De Sarkar, S., Mathew, G., Pande, K., Chauhan, N., Singhvi, A., 2013. Rapid denudation of higher Himalaya during late Pliestocence, evidence from OSL thermochronology. Geochronometria 40 (4), 304–310.
- Delbecq, C.J., Toyozawa, Y., Yuster, P.H., 1974. Tunnelling recombination of trapped electrons and holes in KCI:AgCl and KCI:TiCl. Phys. Rev. B 9 (10), 4497–4505.
- Djimbi, D.M., Gautheron, C., Roques, J., Tassan-Got, L., Gerin, C., Simoni, E., 2015. Impact of apatite chemical composition on (U–Th)/He thermochronometry: an atomistic point of view. Geochim. Cosmochim. Acta 167, 162–176.
- Dodson, M., 1973. Closure temperature in cooling geochronological and petrological systems. Contrib. Mineral. Petrol. 40 (3), 259–274.
- Duller, G.A.T., 1992. Luminescence Chronology of Raised Marine Terraces, South-West North Island, New Zealand. PhD. University of Wales, Aberystwyth.
- Duller, G.A.T., 2015a. Luminescence dating. Encyclopedia of Scientific Dating Methods, pp. 390–404.
- Duller, G.A.T., 2015b. Luminescence, biogenic carbonates. Encyclopedia of Scientific Dating Methods, pp. 445–446.
- Duller, G.A.T., Kook, M., Stirling, R., Roberts, H., Murray, A., 2015. Spatially-resolved thermoluminescence from snail opercula using an EMCCD. Radiat. Meas. 81, 157–162.
- Durcan, J.A., King, G.E., Duller, G.A.T., 2015. DRAC: dose rate and age calculator for trapped charge dating. Quat. Geochronol. 28, 54–61.
- Durrani, S., Amin, Y., 1985. Radiation damage and the anomalous fading of TL in natural and artificial zircons. Nucl. Tracks Radiat. Meas. 10 (4), 539–546.
- Durrani, S.A., Prachyabrued, W., Christodoulides, C., Fremlin, J.H., Edgington, J.A., Chen, R., Blair, I.M., 1972. Thermoluminescence of Apollo 12 samples: implications for lunar temperature and radiation histories. Lunar and Planetary Science Conference Proceedings, p. 2955.
- Durrani, S., Prachyabrued, W., Hwang, F., Edgington, J., Blair, I., 1973. Thermoluminescence of some Apollo 14 and 16 fines and rock samples. Lunar and Planetary Science Conference Proceedings, p. 2465.
- Durrani, S., Khazal, K., Ali, A., 1977. Temperature and duration of the shadow of a recentlyarrived lunar boulder. Nature 266, 411–415.
- Durrani, S., Amin, Y., Alves, J., 1984. Studies of radiation damage in crystals using nucleartrack and thermoluminescence methods. Nucl. Tracks Radiat. Meas. 8 (1), 79–84.
- Duval, M., Guilarte, V., 2015. ESR dosimetry of optically bleached quartz grains extracted from Plio-Quaternary sediment: evaluating some key aspects of the ESR signals associated to the Ti-centers. Radiat. Meas. 78, 28–41.
- Enkelmann, E., Valla, P.G., Champagnac, J.-D., 2015. Low-temperature thermochronology of the Yakutat Plate corner, St. Elias range (Alaska): bridging short-term and longterm deformation. Quat. Sci. Rev. 123, 23–38.
- Finch, A.A., Klein, J., 1999. The causes and petrological significance of cathodoluminescence emissions from alkali feldspars. Contrib. Mineral. Petrol. 135, 234–243.
- Fleming, S.G., 1979. Thermoluminescence Techniques in Archaeology. Clarendon Press, Oxford.
- Gallagher, K., 2012. Transdimensional inverse thermal history modeling for quantitative thermochronology. J. Geophys. Res. Solid Earth 117 (B2).
- Garlick, G.F.J., Robinson, I., 1972. TL of Lunar Samples. In: Runcorn, S.K., Urey, H.C. (Eds.), The Moon, Proceedings from International Astronomical Union Symposium No. 47 Held at the University of Newcastle-Upon-Tyne, England, 22–26 March 1971. Reidel, Dordrecht 324 pp.
- Gautheron, C., Barbarand, J., Ketcham, R.A., Tassan-Got, L., van der Beek, P., Pagel, M., Pinna-Jamme, R., Couffignal, F., Fialin, M., 2013. Chemical influence on α-recoil damage annealing in apatite: implications for (U–Th)/He dating. Chem. Geol. 351, 257–267.
- Gong, G.L., Li, S.H., Sun, W.D., Guo, F., Xia, B., Lü, B.F., 2010. Quartz thermoluminescence—another potential paleo-thermometer for studies of sedimentary basin thermal history. Chin, J. Geophys. 53 (1), 103–112.
- Grün, R., 2001. Trapped charge dating (ESR, TL, OSL). In: Brothwell, D.R., Pollard, A.M. (Eds.), Handbook of Archaeological Sciences. John Wiley & Sons Inc., West Sussex, England, pp. 47–62.

- Grün, R., Tani, A., Gurbanov, A., Koshchug, D., Williams, I., Braun, J., 1999. A new method for the estimation of cooling and denudation rates using paramagnetic centers in quartz: a case study on the Eldzhurtinskiy granite, Caucasus. J. Geophys. Res. Solid Earth 104 (B8), 17531–17549.
- Guenthner, W.R., Reiners, P.W., DeCelles, P.G., Kendall, J., 2014. Sevier belt exhumation in central Utah constrained from complex zircon (U-Th)/He data sets: radiation damage and He inheritance effects on partially reset detrital zircons. Geol. Soc. Am. Bull. B31032. 1.
- Guerin, G., Mercier, N., Adamiec, G., 2011. Dose-rate conversion factors: update. Ancient TL 29 (1), 5–8.
- Guralnik, B., Jain, M., Herman, F., Paris, R.B., Harrison, T.M., Murray, A.S., Valla, P.G., Rhodes, E.J., 2013. Effective closure temperature in leaky and/or saturating thermochronometers. Earth Planet. Sci. Lett. 384, 209–218.
- Guralnik, B., Jain, M., Herman, F., Ankjærgaard, C., Murray, A.S., Valla, P.G., Preusser, F., King, G.E., Chen, R., Lowick, S.E., Kook, M., Rhodes, E.J., 2015a. OSL-thermochronology of feldspar from the KTB borehole, Germany. Earth Planet. Sci. Lett. 423, 232–243.
- Guralnik, B., Ankjærgaard, C., Jain, M., Murray, A.S., Muller, A., Walle, M., Lowick, S.E., Preusser, F., Rhodes, E.J., Wu, T.S., Mathew, G., Herman, F., 2015b. OSLthermochronometry using bedrock quartz: a note of caution. Quat. Geochronol. 25, 37–48
- Guralnik, B., Li, B., Jain, M., Chen, R., Paris, R.B., Murray, A.S., Li, S.-H., Pagonis, V., Valla, P.G., Herman, F., 2015c. Radiation-induced growth and isothermal decay of infrared-stimulated luminescence from feldspar. Radiat. Meas. 81, 224–231.
- Herman, F., Rhodes, E.J., Braun, J., Heiniger, L., 2010. Uniform erosion rates and relief amplitude during glacial cycles in the Southern Alps of New Zealand, as revealed from OSL-thermochronology. Earth Planet. Sci. Lett. 297 (1–2), 183–189.
- Hochman, M.B.M., Ypma, P.J.M., 1988. Changes in the artificial thermoluminescence glow curves of quartz associated with uranium deposits. Int. J. Radiat. Appl. Instrum. Part D 14 (1–2), 105–111.
- Houtermans, F.G., Jäger, E., Schön, M., Stauffer, H., 1957. Messungen der Thermolumineszenz als Mittel zur Untersuchung der thermischen und der Strahlungsgeschichte von natürlichen Mineralien und Gesteinen. Ann. Phys. 20, 283–292
- Hoyt Jr., H.P., Miyajima, M., Walker, R.M., Zimmerman, D.W., Zimmerman, J., Britton, D., Kardos, J.L., 1971. Radiation dose rates and thermal gradients in the lunar regolith: thermoluminescence and DTA of Apollo 12 samples. Lunar and Planetary Science Conference Proceedings, p. 2245.
- Huntley, D.J., 2006. An explanation of the power-law decay of luminescence. J. Phys. Condens. Matter 18 (4), 1359.
- Huntley, D.J., Lamothe, M., 2001. Ubiquity of anomalous fading in K-feldspars and the measurement and correction for it in optical dating. Can. J. Earth Sci. 38 (7), 1093–1106.
- Huntley, D.J., Lian, O.B., 2006. Some observations on tunnelling of trapped electrons in feldspars and their implications for optical dating. Quat. Sci. Rev. 25, 2503–2512.
- Ikeya, M., 1983. ESR studies of geothermal boring cores at Hachobara power station. Jpn. J. Appl. Phys. 22 (12 A), L763.
- Ishii, H., Ikeya, M., Kasuya, M., Furusawa, M., 1991. ESR, TL and FT measurements of a natural apatite. Int. J. Radiat. Appl. Instrum. Part D 18 (1), 189–192.
- Itoh, N., Stoneham, D., Stoneham, A.M., 2002. Ionic and electronic processes in quartz: mechanisms of thermoluminescence and optically stimulated luminescence. J. Appl. Phys. 92, 5036–5044.
- Jain, M., 2009. Extending the dose range: probing deep traps in quartz with 3.06 eV photons. Radiat. Meas. 44 (5), 445–452.
- Jain, M., Ankjærgaard, C., 2011. Towards a non-fading signal in feldspar: insight into charge transport and tunnelling from time-resolved optically stimulated luminescence. Radiat. Meas. 46 (3), 292–309.
- Jain, M., Guralnik, B., Andersen, M.T., 2012. Stimulated luminescence emission from localized recombination in randomly distributed defects. J. Phys. Condens. Matter 24 (38), 385402
- Jain, M., Buylaert, J.P., Thomsen, K.J., Murray, A.S., 2013. Further investigations into "non-fading" in K-feldspar. Quat. Int. 362, 3–7.
- Jain, M., Sohbati, R., Guralnik, B., Murray, A.S., Kook, M., Lapp, T., Prasad, A.K., Thomsen, K.J., Buylaert, J.P., 2015. Kinetics of infrared stimulated luminescence from feldspars. Radiat. Meas. 81, 242–250.
- Kars, R.H., Wallinga, J., Cohen, K.M., 2008. A new approach towards anomalous fading correction for feldspar IRSL dating tests on samples in field saturation. Radiat. Meas. 43 (2–6), 786–790.
- Kasuya, M., Furusawa, M., Ikeya, M., 1990. Distributions of paramagnetic centers and alpha-emitters in a zircon single crystal. Int. J. Radiat. Appl. Instrum. Part D 17 (4), 563–568.
- King, G.E., Finch, A.A., Robinson, R.A.J., Hole, D.E., 2011. The problem of dating quartz 1: Spectroscopic ionoluminescence of dose dependence. Radiat. Meas. 46 (1), 1–9.
- King, G.E., Herman, F., Lambert, R., Valla, P.G., Guralnik, B., 2016a. Multi-OSL thermochronometry of feldspar. Quat. Geochronol. 33, 76–87.
- King, G.E., Herman, F., Guralnik, B., 2016b. Northward migration of the Himalayan syntaxis revealed by OSL thermochronometry. Science 353, 800–804.
- Klasens, H., Wise, M., 1946. Decay of zinc sulphide type phosphors. Nature 158, 483–484. Kohno, H., Yamanaka, C., Ikeya, M., Horino, Y., 1995. Pulsed and CW-ESR study of E' and Al hole centers in quartz produced by irradiations and crushing. Appl. Magn. Reson. 9 (4), 481–489.
- Koshchug, D.G., Solovyov, Y.P., 1998. Accumulation of structural radiation defects in quartz cooling systems: basis for dating. Phys. Chem. Miner. 24 242-24.
- Krbetschek, M.R., Götze, J., Dietrich, A., Trautmann, T., 1997. Spectral information from minerals relevant for luminescence dating. Radiat. Meas. 27, 695–748.
- Kreutzer, S., Schmidt, C., DeWitt, R., Fuchs, M., 2014. The a-value of polymineral fine grain samples measured with the post-IR IRSL protocol. Radiat. Meas. 69, 18–29.

- Lamothe, M., Auclair, M., 1999. A solution to anomalous fading and age shortfalls in optical dating of feldspar minerals. Earth Planet. Sci. Lett. 171 (3), 319–323.
- Lamothe, M., Auclair, M., Hamzaoui, C., Huot, S., 2003. Towards a prediction of long-term anomalous fading of feldspar IRSL Radiat. Meas. 37 (4–5), 493–498.
- Li, B., Li, S.-H., 2011a. Luminescence dating of K-feldspar from sediments: a protocol without anomalous fading correction. Quat. Geochronol. 6 (5), 468–479.
- Li, B., Li, S.-H., 2011b. Thermal stability of infrared stimulated luminescence of sedimentary K-feldspar. Radiat. Meas. 46 (1), 29–36.
- Li, B., Li, S.-H., 2012. Determining the cooling age using luminescence-thermochronology. Tectonophysics 580, 242–248.
- Li, B., Li, S.-H., 2013. The effect of band-tail states on the thermal stability of the infrared stimulated luminescence from K-feldspar. J. Lumin. 136, 5–10.
- Liritzis, I., 2011. Surface dating by luminescence: an overview. Geochronometria 38, 292-302
- Liu, Z., Zhao, H., Wang, C.M., Li, S.H., 2015. Estimation of paleo-firing temperatures using luminescence signals for the volcanic lava baked layer in Datong, China. Quat. Geochronol 30, 363–368
- Liu, J., Murray, A.S., Buylaert, J.P., Jain, M., Chen, J., Lu, Y., 2016. Stability of fine-grained TT-OSL and post-IR IRSL signals from a c. 1 Ma sequence of aeolian and lacustrine deposits from the Nihewan Basin (northern China). Boreas http://dx.doi.org/10.1111/bor.12180.
- Luff, B.J., Townsend, P.D., 1990. Cathodoluminescence of synthetic quartz. J. Phys. Condens. Matter 2, 8089–8097.
- Martini, M., Paleari, A., Spinolo, G., Vedda, A., 1995. Role of [AlO4]° centers in the 380-nm thermoluminescence of quartz. Phys. Rev. B 52, 138.
- Martini, M., Fasoli, M., Galli, A., 2009. Quartz OSL emission spectra and the role of [AlO4]° recombination centres. Radiat. Meas. 44, 458–461.
- McKeever, S.W.S., 1991. Mechanisms of thermoluminescence production: some problems and a few answers? Int. J. Radiat. Appl. Instrum. Part D 18, 5–12.
- Mott, N.F., 1969. Conduction in non-crystalline materials. III. Localised states in a pseudogap and near extremities of conduction and valence bands. Philos. Mag. 19, 835–852.
- Murray, A.S., Wintle, A.G., 2000. Luminescence dating of quartz using an improved singlealiquot regenerative-dose protocol. Radiat. Meas. 32 (1), 57–73.
- Murray, A.S., Wintle, A.G., 2003. The single aliquot regenerative dose protocol: potential for improvements in reliability. Radiat. Meas. 37 (4–5), 377–381.
- Nasdala, L., Grambole, D., Ruschel, K., 2013. Review of effects of radiation damage on the luminescence emission of minerals, and the example of He-irradiated CePO₄. Mineral. Petrol. 107 (3), 441–454.
- Oppermann, F., Tsukamoto, S., 2015. A portable system of X-irradiation and heating for electron spin resonance (ESR) dating. Ancient TL 33 (1), 11–15.
- Pagonis, V., Morthekai, P., Kitis, G., 2014. Kinetic analysis of thermoluminescence glow curves in feldspar: evidence for a continuous distribution of energies. Geochronometria 41 (2), 168–177.
- Perny, B., Eberhardt, P., Ramseyer, K., Mullis, J., Pankrath, R., 1992. Microdistribution of Al, Li, and Na in quartz: possible causes and correlation with short-lived cathodoluminescence. Am. Mineral. 77, 534–544.
- Polymeris, G.S., Giannoulatou, V., Sfampa, I.K., Tsirliganis, N.C., Kitis, G., 2014. Search for stable energy levels in materials exhibiting strong anomalous fading: the case of apatites. J. Lumin. 153, 245–251.
- Poolton, N.R.J., Kars, R.H., Wallinga, J., Bos, A.J.J., 2009. Direct evidence for the participation of band-tails and excited-state tunnelling in the luminescence of irradiated feldspars. J. Phys. Condens. Matter 21 (48), 485505.
- Preusser, F., Chithambo, M.L., Gotte, T., Martini, M., Ramseyer, K., Sendezera, E.J., Susino, G.J., Wintle, A.G., 2009. Quartz as a natural luminescence dosimeter. Earth-Sci. Rev. 97, 184–214.
- Prokein, J., Wagner, G.A., 1994. Analysis of thermoluminescent glow peaks in quartz derived from the KTB-drill hole. Radiat. Meas. 23 (1), 85–94.
- Qin, J., Chen, J., Valla, P.G., Herman, F., Li, K., 2015. Estimating rock cooling rates by using multiple luminescence thermochronometers. Radiat. Meas. 79, 13–18.
- Reiners, P.W., Ehlers, T.A., 2005. Low-temperature thermochronology: techniques, interpretations, and applications. Rev. Mineral. Geochem. 58 620 pp..
- Richter, D., Richter, A., Dornich, K., 2013. Lexsyg a new system for luminescence research. Geochronometria 40 (4), 220–228.
- Rink, W.J., 1994. Billion-year age dependence of luminescence in granitic quartz. Radiat. Meas. 23 (2–3), 419–422.
- Rink, W.G., 1997. Electron spin resonance (ESR) dating and ESR applications in quaternary science and archaeology. Radiat. Meas. 27 (5–6), 975–1025.
- Roberts, H.M., 2007. Assessing the effectiveness of the double-SAR protocol in isolating a luminescence signal dominated by quartz. Radiat. Meas. 42 (10), 1627–1636.
- Roberts, R.G., Lian, O.B., 2015. Dating techniques: illuminating the past. Nature 520, 438–439.
- Ronca, L., 1964. Minimum length of time of frigid conditions in Antarctica as determined by thermoluminescence. Am. J. Sci. 262 (6), 767–781.
- Ronca, L.B., Zeller, E.J., 1965. Thermoluminescence as a function of climate and temperature. Am. J. Sci. 263 (5), 416–428.
- Scherer, T., Agel, A., Hafner, S.S., 1993. Determination of uplift rates using ESR investigations of quartz, KTB Rep. 93-2. Kontinentales Tiefbohrprogram der Bundesrepublic Deutschland Niedersächs. Landesamt Bodenforsch, Hannover, pp. 121–124.
- Schmidt, C., Friedrich, J., Zöller, L., 2015. Thermochronometry using red TL of quartz? numerical simulation and observations from in-situ drill-hole samples. Radiat. Meas. 81, 98–103.
- Shulgin, B., Fedorovskikh, Y.A., Krasnobaev, A.A., Polezhaev, Y.M., 1974. The thermostimulated luminescence of natural zircon. Zh. Prikl. Spektrosk. 21 (3), 470–474.

- Shuster, D.L., Cassata, W.S., 2015. Paleotemperatures at the lunar surfaces from open system behavior of cosmogenic 38 Ar and radiogenic 40 Ar. Geochim. Cosmochim. Acta 155, 154–171.
- Shuster, D.L., Flowers, R.M., Farley, K.A., 2006. The influence of natural radiation damage on helium diffusion kinetics in apatite. Earth Planet. Sci. Lett. 249, 148–161.
- Skinner, A.R., 2011, Current topics in ESR dating, Radiat, Meas, 46 (9), 749–753.
- Skinner, A.R., 2015. Electron spin resonance (ESR) dating, general principles. In: Rink, W.J., Thompson, J.W. (Eds.), Encyclopedia of Scientific Dating Methods. Springer.
- Sohbati, R., 2015. Luminescence, rock surfaces. Encyclopedia of Scientific Dating Methods, pp. 485–488.
- Sohbati, R., Murray, A., Jain, M., Thomsen, K., Hong, S.C., Yi, K., Choi, J.H., 2013. Na-rich feld-spar as a luminescence dosimeter in infrared stimulated luminescence (IRSL) dating. Radiat. Meas. 51, 67–82.
- Spooner, N.A., 1994. The anomalous fading of infra-red stimulated luminescence from feldspars. Radiat. Meas. 23, 625–632.
- Stirling, R., Duller, G., Roberts, H., 2012. Developing a single-aliquot protocol for measuring equivalent dose in biogenic carbonates. Radiat. Meas. 47 (9), 725–731.
- Takashima, I., 1979. Preliminary study on the determination of alteration age by a thermoluminescence method. Bull. Geol. Surv. Jpn 30, 285–295.
- Takashima, I., 1985. Thermoluminescence dating of volcanic rocks and alteration minerals and their application to geothermal history. Bull. Geol. Surv. Jpn 36, 321–366.
- Templer, R.H., 1985. The removal of anomalous fading in zircon. Nucl. Tracks Radiat. Meas. 10 (4–6), 531–537.
- Templer, R.H., 1986. Auto-regenerative TL dating of zircon inclusions. Radiat. Prot. Dosim. 17 (1-4), 235–239.
- Thomsen, K.J., Murray, A.S., Jain, M., Bøtter-Jensen, L., 2008. Laboratory fading rates of various luminescence signals from feldspar-rich sediment extracts. Radiat. Meas. 43 (9), 1474–1486
- Thomsen, K.J., Murray, A.S., Bøtter-Jensen, L., 2005. Sources of variability in OSL dose measurements using single grains of quartz. Radiat. Meas. 1 (39), 47–61.
- Timar-Gabor, A., Wintle, A.G., 2013. On natural and laboratory generated dose response curves for quartz of different grain sizes from Romanian loess. Quat. Geochronol. 18, 34–40.
- Toyoda, S., Ikeya, M., 1991. Thermal stabilities of paramagnetic defect and impurity centers in quartz: basis for ESR dating of thermal history. Geochem. J. 25 (6), 437–445.
- Toyoda, S., Rink, W., Yonezawa, C., Matsue, H., Kagami, T., 2001. In situ production of alpha particles and alpha recoil particles in quartz applied to ESR studies of oxygen vacancies. Quat. Sci. Rev. 20 (5), 1057–1061.
- Tremblay, M.M., Shuster, D.L., Balco, G., 2014. Cosmogenic noble gas paleothermometry. Earth Planet. Sci. Lett. 400, 195–205.
- Tsuchiya, N., Fujino, K., 2000. Evaluation of cooling history of the quaternary Takidani pluton using thermoluminescence technique. Proceedings of World Geothermal Congress, pp. 3939–3944.
- Tsukamoto, S., 2015. Luminescence, volcanic rocks. Encyclopedia of Scientific Dating Methods, pp. 493–495.
- Tsukamoto, S., Murray, A.S., Huot, S., Watanuki, T., Denby, P.M., Bøtter-Jensen, L., 2007. Luminescence property of volcanic quartz and the use of red isothermal TL for dating tephras. Radiat. Meas. 42 (2), 190–197.
- Tsukamoto, S., Duller, G.A.T., Wintle, A.G., Frechen, M., 2010. Optical dating of a Japanese marker tephra using plagioclase. Quat. Geochronol. 5, 274–278.
- Tsukamoto, S., Duller, G.A.T., Wintle, A.G., Muhs, D., 2011. Assessing the potential for luminescence dating of basalts. Quat. Geochronol. 6, 61–70.
- Tsukamoto, S., Kataoka, K., Oguchi, T., Murray, A.S., Komatsu, G., 2014. Luminescence dating of scoria fall and lahar deposits from Somma–Vesuvius, Italy. Quat. Geochronol. 20, 39–50.
- Tsukamoto, S., Toyoda, S., Tani, A., Oppermann, F., 2015. Single aliquot regenerative dose method for ESR dating using X-ray irradiation and preheat. Radiat. Meas. 81, 9–15.
- Valla, P.G., Lowick, S.E., Herman, F., Champagnac, J.-D., Steer, P., Guralnik, B., 2016. Exploring IRSL₅₀ fading variability in bedrock feldspars and implications for OSL thermochronometry. Quat. Geochronol. http://dx.doi.org/10.1016/j.quageo.2016.08. 004 in press.
- Vandenberghe, D., De Corte, F., Buylaert, J.P., Kučera, J., 2008. On the internal radioactivity in quartz. Radiat. Meas. 43 (2), 771–775.
- Vaz, J., Senftle, F., 1971. Geologic age dating of zircon using thermoluminescence. Mod. Geol. 2, 239–245.
- Visocekas, R., Ceva, T., Marti, C., 1976. Tunneling processes in afterglow of calcite. Phys. Status Solidi A 35 (1), 315–327.
- von Neumann, J., 1951. Various techniques used in connection with random digits. Monte Carlo methods. Natl. Bur. Stand. 12, 36–38.
- Walker, R.M., Zimmerman, D.W., Zimmerman, J., 1972. Thermoluminescence of lunar samples: measurement of temperature gradients in core material. Moon 4 (3–4), 308–314.
- Walther, R., Zilles, D., 1994. ESR studies on bleached sedimentary quartz. Quat. Geochronol. 13, 611–614.
- Wang, X.L., Wintle, A.G., Lu, Y.C., 2006. Thermally transferred luminescence in fine-grained quartz from Chinese loess: basic observations. Radiat. Meas. 41 (6), 649–658.
- Wauschkuhn, B., Jonckheere, R., Ratschbacher, L., 2015. The KTB apatite fission-track profiles: building on a firm foundation? Geochim. Cosmochim. Acta 167, 27–62.
- Wintle, A.G., 1973. Anomalous fading of thermoluminescence in mineral samples. Nature 245. 143–144.
- Wintle, A.G., 2008. Luminescence dating: where it has been and where it is going. Boreas 37 (4), 471–482.
- Wintle, A.G., Murray, A.S., 2006. A review of quartz optically stimulated luminescence characteristics and their relevance in single-aliquot regeneration dating protocols. Radiat. Meas. 41 (4), 369–391.

- Wu, T.-S., Jain, M., Guralnik, B., Murray, A.S., Chen, Y.-G., 2015. Luminescence characteristics of quartz from Hsuehshan range (Central Taiwan) and implications for thermochronometry. Radiat. Meas. 81, 104–109.

 Yang, H., McKeever, S.W.S., 1990. The pre-dose effect in crystalline quartz. J. Phys. D. Appl. Phys. 23, 237.
- Pnys. 23, 23/.
 Yokoyama, Y., Falgur es, C., Quaegebeur, J.P., 1985. ESR dating of sediment baked by lava flows: comparison of paleo-doses for Al and Ti centers. In: Ikeya, M., Miki, T. (Eds.), ESR Dating and Dosimetry. Ionics, Tokyo, pp. 197–204.
 Ypma, P.J., Hochman, M.B., 1991. Thermoluminescence geothermometry a case study of the Otway Basin. APEA J. 35, 312–324.
- Zeitler, P.K., Meltzer, A.S., Brown, L., Kidd, W.S., Lim, C., Enkelmann, E., 2014. Tectonics and topographic evolution of Namche Barwa and the easternmost Lhasa block, Tibet.
- Geol. Soc. Am. Spec. Pap. 507 SPE507-02.

 Zeller, A., 1968. Influence of microclimate upon TL of rock. In: McDougall, D.J. (Ed.), TL of Geologic Materials. Academic Press, pp. 507–518.

 Zeller, E., Ronca, L., 1963. Reversible and irreversible thermal effects on the thermolumi-
- nescence of limestone. Earth Sci. Meteor. 281–294.